Atmos. Chem. Phys., 16, 13853–13884, 2016
www.atmos-chem-phys.net/16/13853/2016/
doi:10.5194/acp-16-13853-2016


Atmospheric Chemistry and Physics
Open Access
EGU

# Spatiotemporal variability and contribution of different aerosol types to the aerosol optical depth over the Eastern Mediterranean

**Aristeidis K. Georgoulias[1,2,3,a], Georgia Alexandri[4,5], Konstantinos A. Kourtidis[5], Jos Lelieveld[3,6], Prodromos Zanis[1], Ulrich Pöschl[2], Robert Levy[7], Vassilis Amiridis[8], Eleni Marinou[4,8], and Athanasios Tsikerdekis[1]**

[1]Department of Meteorology and Climatology, School of Geology, Aristotle University of Thessaloniki, 54124 Thessaloniki, Greece
[2]Multiphase Chemistry Department, Max Planck Institute for Chemistry, 55128 Mainz, Germany
[3]Energy, Environment and Water Research Center, The Cyprus Institute, Nicosia, Cyprus
[4]Laboratory of Atmospheric Physics, Physics Department, Aristotle University of Thessaloniki, 54124 Thessaloniki, Greece
[5]Laboratory of Atmospheric Pollution and Pollution Control Engineering of Atmospheric Pollutants, Department of Environmental Engineering, Democritus University of Thrace, 67100 Xanthi, Greece
[6]Atmospheric Chemistry Department, Max Planck Institute for Chemistry, 55128 Mainz, Germany
[7]Earth Science Division, NASA Goddard Space Flight Center, Greenbelt, MD 20771, USA
[8]Institute for Astronomy, Astrophysics, Space Application and Remote Sensing, National Observatory of Athens, 15236 Athens, Greece
[a]current address: Laboratory of Atmospheric Pollution and Pollution Control Engineering of Atmospheric Pollutants, Department of Environmental Engineering, Democritus University of Thrace, 67100 Xanthi, Greece

*Correspondence to:* Aristeidis K. Georgoulias (argeor@env.duth.gr)

Received: 11 May 2016 – Published in Atmos. Chem. Phys. Discuss.: 11 July 2016
Revised: 15 October 2016 – Accepted: 17 October 2016 – Published: 9 November 2016

**Abstract.** This study characterizes the spatiotemporal variability and relative contribution of different types of aerosols to the aerosol optical depth (AOD) over the Eastern Mediterranean as derived from MODIS (Moderate Resolution Imaging Spectroradiometer) Terra (March 2000–December 2012) and Aqua (July 2002–December 2012) satellite instruments. For this purpose, a $0.1° \times 0.1°$ gridded MODIS dataset was compiled and validated against sun photometric observations from the AErosol RObotic NETwork (AERONET). The high spatial resolution and long temporal coverage of the dataset allows for the determination of local hot spots like megacities, medium-sized cities, industrial zones and power plant complexes, seasonal variabilities and decadal averages. The average AOD at 550 nm ($AOD_{550}$) for the entire region is $\sim 0.22 \pm 0.19$, with maximum values in summer and seasonal variabilities that can be attributed to precipitation, photochemical production of secondary organic aerosols, transport of pollution and smoke from biomass burning in central and eastern Europe and transport of dust from the Sahara and the Middle East. The MODIS data were analyzed together with data from other satellite sensors, reanalysis projects and a chemistry–aerosol-transport model using an optimized algorithm tailored for the region and capable of estimating the contribution of different aerosol types to the total $AOD_{550}$. The spatial and temporal variability of anthropogenic, dust and fine-mode natural aerosols over land and anthropogenic, dust and marine aerosols over the sea is examined. The relative contribution of the different aerosol types to the total $AOD_{550}$ exhibits a low/high seasonal variability over land/sea areas, respectively. Overall, anthropogenic aerosols, dust and fine-mode natural aerosols account for $\sim 51$, $\sim 34$ and $\sim 15$ % of the total $AOD_{550}$ over land, while, anthropogenic aerosols, dust and marine aerosols account $\sim 40$, $\sim 34$ and $\sim 26$ % of the total $AOD_{550}$ over the sea, based on MODIS Terra and Aqua observations.

**Published by Copernicus Publications on behalf of the European Geosciences Union.**

## 1 Introduction

For more than 15 years, two MODIS (Moderate Resolution Imaging Spectroradiometer) satellite sensors have been monitoring tropospheric aerosols at a global scale on a daily basis. The retrieved aerosol optical properties have been used in numerous air quality studies as well as studies related to the effect of airborne particles on various climatic parameters (e.g., radiation, clouds, precipitation). The $1^\circ \times 1^\circ$ daily gridded level-3 dataset is primarily used for global as well as regional studies, while the single-pixel level-2 data with a 10 km resolution (at nadir) are mostly used for regional and local scale studies. Nevertheless, the use of the coarse-resolution MODIS data has predominated, even in regional studies. The reasons for this could be the smaller file size, which makes their processing and storage easier, or the fact that they are easily accessible through user-friendly databases, which also allow for a very basic analysis like e.g., NASA's GIOVANNI website (http://giovanni.gsfc.nasa.gov/giovanni/) (Acker and Leptoukh, 2007).

The same holds for studies focusing on the Mediterranean Basin, an area which is considered of particular sensitivity as far as air pollution and climate change is concerned (Lelieveld et al., 2002; Giorgi, 2006). The Mediterranean Basin is one of the regions with the highest aerosol optical depths (AODs) in the world (Husar et al., 1997; Ichoku et al., 2005; Papadimas et al., 2008), causing significant climate forcing especially in summer, which is characterized by low cloudiness and high incoming solar radiation levels (Papadimas et al., 2012; Alexandri et al., 2015). The Mediterranean is also recognized as a crossroads between three continents where aerosols of various types accumulate (Lelieveld et al., 2002). Marine aerosols from the Mediterranean Sea and even the Atlantic Ocean combine with aerosols from continental Europe (urban and rural), dust particles transported from the Sahara and Middle East, as well as biomass burning aerosols from occasional wild fires and agricultural burning (Lelieveld et al., 2002). Specifically, as discussed in Hatzianastassiou et al. (2009), the Eastern Mediterranean, the region under investigation here, is located at a key point of this crossroads. There is a significant number of ground- and satellite-based studies on the abundance and optical properties of tropospheric aerosols in the area; however, these studies are either focused on specific spots, or they used a coarse spatial and temporal resolution.

The ground-based instrumentation used in studies focusing on the aerosol load and optical properties over the Eastern Mediterranean includes active and passive sensors such as lidars (e.g., Papayannis and Balis, 1998; Balis et al., 2004; Papayannis et al., 2005, 2009; Amiridis et al., 2005, 2009; Mamouri et al., 2013; Kokkalis et al., 2013; Nisantzi et al., 2015), Cimel sun photometers (e.g., Israelevich et al., 2003; Kubilay et al., 2003; Derimian et al., 2006; Kalivitis et al., 2007; Kelektsoglou and Rapsomanikis, 2011; Nikitidou and Kazantzidis, 2013), Brewer spectrophotometers (e.g., Kazadzis et al., 2007; Koukouli et al., 2010), Multi-Filter Radiometers (e.g., Gerasopoulos et al., 2009, 2011; Kazadzis et al., 2014), ceilometers (e.g., Tsaknakis et al., 2011), Microtops sun photometers (e.g., El-Metwally and Alfaro, 2013), etc. However, these and other studies not referenced here either refer to specific spots with the majority of the ground stations being situated in large urban centers (e.g., Athens, Thessaloniki, Cairo) or to specific events (e.g., Sahara dust intrusions, biomass burning events).

On the other hand, AOD and other aerosol optical properties have been studied over the greater Eastern Mediterranean region based on data from Meteosat (Moulin et al., 1998), SeaWIFS (Koren et al., 2003; Antoine and Nobileau, 2006; Mélin et al., 2007; Nabat et al., 2013), TOMS (Alpert and Ganor, 2001; Israelevich et al., 2002; Koukouli et al., 2006, 2010; Hatzianastassiou et al., 2009; Israelevich et al., 2012, Kaskaoutis et al., 2012a; Nabat et al., 2013; Gkikas et al., 2013, 2014; Varga et al., 2014), MODIS Terra and Aqua (Barnaba and Gobbi, 2004; Papayannis et al., 2005; Kaskaoutis et al., 2007, 2008, 2010, 2011, 2012a, b, c, d; Kosmopoulos et al., 2008; Papadimas et al., 2008, 2009; Rudich et al., 2008; Carmona and Alpert, 2009; Karnieli et al., 2009; Gkikas et al., 2009, 2013; Hatzianastassiou et al., 2009; El-Metwally et al., 2010; Koukouli et al., 2010; Kanakidou et al., 2011; Gerasopoulos et al., 2011; de Meij and Lelieveld, 2011; Marey et al., 2011; de Meij et al., 2012; Nabat et al., 2012, 2013; Nikitidou and Kazantzidis, 2013; Athanassiou et al., 2013; Benas et al., 2011, 2013; Sorek-Hamer et al., 2013; Kabatas et al., 2014; Kourtidis et al., 2014; Mishra et al., 2014; Flaounas et al., 2015; Kloog et al., 2015), OMI/AURA (Kaskaoutis et al., 2010; El-Metwally et al., 2010; Marey et al., 2011; Kaskaoutis et al., 2012b, c, Gkikas et al., 2013, 2014; Sorek-Hamer et al., 2013; Varga et al., 2014; Flaounas et al., 2015), CALIOP/CALIPSO (Amiridis et al., 2009, 2013, Mamouri et al., 2009; Marey et al., 2011; Kaskaoutis et al., 2012c; de Meij et al., 2012; Nabat et al., 2012, 2013; Mamouri and Ansmann, 2015), MISR/Terra (Kanakidou et al., 2011; Marey et al., 2011; de Meij and Lelieveld, 2011; de Meij et al., 2012; Nabat et al., 2013; Kabatas et al., 2014; Abdelkader et al., 2015), as well as NOAA/AVHRR, MERIS/ENVISAT, AATSR/ENVISAT, PARASOL/POLDER, MSG/SEVIRI and Landsat satellite data (see Retalis and Sifakis, 2010; Nabat et al., 2013; Benas et al., 2013; Sifakis et al., 2014). To our knowledge, these studies comprise the majority of works focusing on tropospheric aerosols over the Eastern Mediterranean by means of satellite remote sensing, published in peer-reviewed journals the last $\sim$ 15 years. As shown in Fig. 4 of this work, the publication rate of satellite-based studies focusing on the Eastern Mediterranean aerosols nearly doubled every 3 years during the period 1997–2014, which is indicative of the increasing scientific interest in the area.

In a very large fraction of the satellite-based studies referenced above, the data used are either of coarse mode (usually 1°, which is $\sim$ 100 km for the midlatitudes) or focus on

specific spots for validation purposes. In a few cases, high-resolution data were used in spatiotemporal studies; however, either these studies are restricted over surfaces covered by water, or examine a short period only. For example, Moulin et al. (1998) investigated the dust AOD patterns over the oceanic areas of the Mediterranean Basin at a resolution of $35 \times 35\,km^2$ for a period of 11 years (1984–1994) using Meteosat observations. A 7-year climatology (1998–2004) of total and dust AOD for the same regions at a resolution of $0.16° \times 0.16°$ was compiled by Antoine and Nobileau (2006) using observations from SeaWIFS. Mélin et al. (2007) merged SeaWIFS and MODIS data and presented high-resolution AOD patterns ($2 \times 2\,km^2$) for May 2003. As far as MODIS is concerned, only Barnaba and Gobbi (2004) presented a high-resolution ($0.1° \times 0.1°$) spatiotemporal analysis for a period of 1 year (2001) over sea only. In a recent paper, Athanassiou et al. (2013) presented, in detail, a method for compiling a 0.5° resolution AOD gridded dataset using level-2 MODIS Terra data for the greater region of Greece (2000–2008). However, the spatial resolution they used ($\sim 50$ km) is not high enough to reveal local sources (e.g., cities, islands, river banks). Overall, there has so far not been any detailed high-resolution spatiotemporal study of the AOD over the Eastern Mediterranean.

In this paper, the $AOD_{550}$ spatiotemporal variability over the Eastern Mediterranean (30–45° N, 17.5–37.5° E) is presented at a high spatial resolution ($0.1° \times 0.1°$) based on MODIS Terra and Aqua observations. Level-2 MODIS data are used for the compilation of a 0.1° gridded dataset, which is validated against ground-based observations. In order to calculate the contribution of different aerosol types to the total AOD, the MODIS data were analyzed together with other satellite data, ERA-Interim and MACC reanalysis data and the Goddard Chemistry Aerosol Radiation and Transport (GOCART) model, using an algorithm optimized for the surface properties of the Eastern Mediterranean region. The different datasets used in this research are presented in detail in Sect. 2, while a detailed description of the method is given in Sect. 3. Sect. 4 includes the results from the MODIS validation procedure, the annual and seasonal variability of $AOD_{550}$ over the region with a discussion on the local aerosol sources and the differences between Terra and Aqua and the annual and seasonal contribution of different aerosol types to the total $AOD_{550}$. Finally, in Sect. 5, the main conclusions of the paper are presented along with a short discussion on how these results could contribute to future studies in the area.

## 2 Observations, reanalysis data and model simulations

### 2.1 MODIS Terra and Aqua satellite observations

The main data used in this work come from the level-2 MODIS Terra (MOD04_L2) and MODIS Aqua (MYD04_L2) Collection 051 dataset and have been acquired through NASA's Level 1 and Atmosphere Archive and Distribution System (LAADS) (http://ladsweb.nascom.nasa.gov). MODIS Terra and Aqua have a daytime Equator crossing time at 10:30 LT (morning) and 13:30 LT (noon), respectively. MODIS instruments, with a viewing swath of 2330 km, measure backscattered radiation at 36 spectral bands between 0.415 and 14.235 µm with a spatial resolution of 250, 500 and 1000 m, providing a nearly global coverage on a daily basis. Aerosol optical properties for the standard MODIS aerosol product are retrieved using two different "Dark Target" (DT) algorithms. One is used over land surfaces (Kaufman et al., 1997; Levy et al., 2007a, b, 2010; Remer et al., 2005), and the other over oceanic regions (Tanré et al., 1997; Levy et al., 2003; Remer et al., 2005). The "Deep Blue" algorithm (DB) (Hsu et al., 2004, 2006) has been used for retrievals over bright land surfaces (e.g., deserts) where the DT algorithm fails. Only recently did updates to the algorithm allow for extending the spatial coverage of the DB aerosol product over all land areas (Hsu et al., 2013; Sayer et al., 2013, 2014). AErosol RObotic NETwork (AERONET) Cimel sun photometric measurements have been extensively used for the validation of the MODIS over-land and over-ocean products (e.g., Chu et al., 2002; Remer et al., 2002, 2005; Levy et al., 2010; Shi et al., 2013).

In this work, $AOD_{550}$ over both land and sea and the fine mode ratio ($FMR_{550}$) over sea from Collection 051 were used at a spatial resolution of 10 km (at nadir). The uncertainty of the MODIS aerosol optical depth has been estimated at $\pm(0.05 + 0.15\,AOD)$ over land (Chu et al., 2002; Levy et al., 2010) and $\pm(0.03 + 0.05\,AOD)$ over ocean (Remer et al., 2002) relative to the AERONET AOD. Specifically, for the DT data used in this work, only high-quality retrievals are used over land. This means that the data have a quality assurance confidence (QAC) flag equal to 3 (high confidence). For retrievals over sea we use data with a QAC flag of 1 (marginally good), 2 (good) and 3 (see Levy et al., 2009 for details). The pre-launch uncertainty of $FMR_{550}$ is ±30 % over ocean (Remer et al., 2005), while over land this parameter is by no means trustworthy and should only be used in qualitative studies (e.g., see Georgoulias and Kourtidis, 2011). In cases where the DT algorithm does not provide products over land, especially over bright arid and semi-arid regions of northern Africa, $AOD_{550}$ values from the DB algorithm are used in our work. The expected uncertainty of the DB product used here is $\pm(0.05+0.2\,AOD)$ relative to the AERONET AOD (Hsu et al., 2006). The analyzed datasets cover the period from March 2000 to December 2012 for Terra and from July 2002 to December 2012 for Aqua MODIS, covering the region of the Eastern Mediterranean. The Collection 051 DB data for Terra are only available until December 2007 due to calibration issues; nevertheless, these data are carefully used within our analysis to obtain a complete image of the aerosol load over the region.

### 2.2 AERONET ground-based observations

For the evaluation of the MODIS $AOD_{550}$, version 2.0 level 2.0 high-quality cloud-screened data from 13 AERONET Cimel network ground stations in the region of the Eastern Mediterranean have been acquired (http://aeronet.gsfc.nasa.gov). The stations were selected such that their operation period covers at least 2 years and there are at least 100 common days of co-localized AERONET and MODIS observations. AERONET Cimel sun photometers measure solar radiation every 15 min within the spectral range from 340 to 1020 nm (Holben et al., 2001). The spectral measurements allow for the retrieval of columnar aerosol properties (see Holben et al., 1998; Dubovik and King, 2000; Dubovik et al., 2000, 2002). The AERONET AOD uncertainty is on the order of 0.01–0.02 (Eck et al., 1999), being larger at shorter wavelengths. Here, we use quadratic fits on a log–log scale to interpolate the AERONET data (AODs at 440, 500, 675 and 870 nm) to the MODIS band-effective wavelength of 550 nm (Eck et al., 1999; Levy et al., 2010). Therefore, we can directly compare the MODIS $AOD_{550}$ retrievals against AERONET observations. Simultaneous measurements of the Ångström Exponent (AE) for the spectral range 440–870 nm ($AE_{440–870}$) from the 13 AERONET stations mentioned above were also utilized in this work in order to account for days with dust dominance. The uncertainty of the AE is significantly higher than the AOD uncertainty, especially under low AOD conditions. Li et al. (2014) found that the uncertainty for a typical northern hemispheric AERONET station (GSFC) is $\sim 0.6$ during winter, when AODs are significantly lower compared to summer ($\sim 0.15$).

### 2.3 LIVAS CALIOP/CALIPSO dust climatology

Dust aerosol optical depths at 532 nm ($AOD_{532}$) from CALIOP/CALIPSO (Cloud-Aerosol Lidar with Orthogonal Polarization instrument aboard Cloud-Aerosol Lidar and Infrared Pathfinder Satellite Observations satellite) at a resolution of $1^\circ \times 1^\circ$ are also used here for the period 2007–2012. CALIPSO measures cloud and aerosol properties flying at a 705 km sun synchronous polar orbit with a 16-day repeat cycle and an Equator crossing time close to that of the Aqua satellite (13:30 LT). The dust product used here comes from a Saharan-dust-optimized retrieval scheme that was developed within the framework of the LIVAS (Lidar Climatology of Vertical Aerosol Structure for Space-Based LIDAR Simulation Studies) project (Amiridis et al., 2015), and has been presented in detail in Amiridis et al. (2013). In brief, the LIVAS dust product is optimized for Europe by applying a lidar ratio of 58 sr instead of 40 sr to Level 2 dust-related backscatter products. This correction results in an improvement of the $AOD_{532}$ product. Comparison against spatially and temporally co-located AERONET observations (Amiridis et al., 2013) returned an absolute bias of $\sim -0.03$. The corresponding reported biases for the original CALIPSO data are significantly higher ($\sim -0.10$). The bias is even lower when compared against MODIS satellite-based observations. Other improvements of this product are related to the use of a new methodology for the calculation of pure dust extinction from dust mixtures and the application of an averaging scheme that includes zero extinction values for the non-dust aerosol types detected. Overall, this product (hereafter denoted as LIVAS dust product) exhibits better agreement with observations from MODIS and AERONET and simulations from the BSC-DREAM8b dust model over northern Africa and Europe than the standard CALIPSO data; hence it is an ideal tool for the evaluation of other satellite-based products.

### 2.4 Earth Probe TOMS and OMI satellite observations

For this work, ultraviolet (UV) Aerosol Index (AI) data (Herman et al., 1997) from the Earth Probe TOMS (Total Ozone Mapping) spectrometer aboard Earth Probe for the period January 2000–September 2004 at a resolution of $1^\circ$ (latitude) $\times 1.25^\circ$ (longitude) and the OMI (Ozone Monitoring Instrument) sensor aboard EOS AURA for the period October 2004–December 2012 at a resolution of $1^\circ \times 1^\circ$ were acquired through the GIOVANNI web database (http://giovanni.gsfc.nasa.gov/giovanni/). Earth Probe TOMS continued the record of the first three TOMS instruments aboard Nimbus-7, Meteor-3 and ADEOS flying in a sun synchronous orbit at an altitude of 740 km with an instantaneous field of view size of $39 \times 39\,km^2$ at nadir. The instrument had an ascending node Equator crossing time at 12:00 LT, covering 85 % of the globe on a daily basis from July 1996 until December 2005. The satellite was originally set to a 500 km sun synchronous orbit, but was set to its final orbit after the failure of ADEOS satellite in June 1997. OMI is a UV–VIS (ultraviolet–visible) nadir solar backscatter spectrometer (Levelt et al., 2006) that continues the long TOMS record. OMI flies in a sun synchronous polar orbit at an altitude of 705 km with an ascending node Equator crossing time at 13:45 LT. Its 2600 km viewing swath allows for almost daily global coverage, while the spatial resolution of the instrument is $13 \times 24\,km^2$ at nadir. The AI (also known as Absorbing Aerosol Index), which is calculated by the two instruments, constitutes a qualitative indicator of the presence of UV absorbing aerosols in the atmosphere such as biomass burning and dust (Torres et al., 1998). Positive AI values generally represent absorbing aerosols, while small or negative values represent non-absorbing aerosols. The Version 8 algorithm is applied to spectral measurements from both TOMS and OMI sensor to produce a consistent long-term AI time series (Li et al., 2009). AI is calculated from the difference in surface reflectivity derived from the 331.2 and 360 nm measurements, exhibiting an uncertainty of $\pm 30$ % (Torres et al., 2007).

### 2.5 ERA-Interim reanalysis data

Wind speed (ws) data at 10 m above surface from the ERA-Interim reanalysis (Dee et al., 2011) are used for 09:00 and 12:00 UTC on a daily basis for the period 2000–2012. We use 09:00 and 12:00 UTC data in order to be closer to the Terra and Aqua overpass time in the area, respectively. The various ERA-Interim reanalysis fields are produced by ECMWF's Integrated Forecast System (IFS) assimilating satellite- and ground-based observations. The system includes a 4-D variational analysis with a 12 h analysis window. The spatial resolution of the ERA-Interim data is $\sim 79$ km, with 60 vertical levels from the surface up to 0.1 hPa, while the data can be acquired at various resolutions (in this work $1^\circ \times 1^\circ$) through ECMWF's website (http://apps.ecmwf.int/datasets/data/interim-full-daily/). Over ocean, the 10 m ERA-Interim wind speed exhibits a bias of less than $-0.5\,\mathrm{m\,s^{-1}}$ compared to quality-controlled in situ observations on a global scale (Dee et al., 2011). Specifically, for the region of the Eastern Mediterranean examined here, the 10 m ERA-Interim wind speed exhibits a bias of $-0.96\,\mathrm{m\,s^{-1}}$ ($-16\,\%$) compared to satellite-based observations from QuikSCAT (Herrmann et al., 2011).

### 2.6 MACC reanalysis data

The daily MACC total and dust $AOD_{550}$ data for the period 2003–2012 come from the aerosol analysis and forecast system of ECMWF, which consists of a forward model (Morcrette et al., 2009) and a data-assimilation module (Benedetti et al., 2009). $AOD_{550}$ measurements from the two MODIS instruments aboard Terra and Aqua are assimilated by the MACC forecasting system through a 4D-Var assimilation algorithm to produce the aerosol analysis, leading to an improved AOD representation compared to observations (see Benedetti et al., 2009; Mangold et al., 2011). Five aerosol species are included within MACC, namely, mineral dust, sea salt, sulfates, black carbon and organic matter. Three different sized bins are used for mineral dust and sea salt particles, while the black carbon and organic material are distributed to a hydrophilic and a hydrophobic mode. Dust and sea salt emissions are given as a function of surface wind speed, while the emissions of the other species are taken from inventories. The spatial resolution of the MACC reanalysis data is $\sim 79$ km with 60 vertical levels from the surface up to 0.1 hPa and can be acquired from http://apps.ecmwf.int/datasets/data/macc-reanalysis/ for the period 2003–2012. The MACC total and dust AODs have been evaluated against ground- and satellite-based observations (see Elguindi et al., 2010; Bellouin et al., 2013; Inness et al., 2013; Cesnulyte et al., 2014; Cuevas et al., 2015), showing that the MACC aerosol products generally capture the daily, seasonal and interannual variability of aerosols well. As discussed in Bellouin et al. (2013) the uncertainties of MACC total $AOD_{550}$ ($\sim 0.03$) and dust $AOD_{550}$ ($\sim 0.014$) arise from uncertainties in the MODIS retrievals, which are assimilated into the model and errors in the forward modeling of total and component AODs.

### 2.7 GOCART data

Daily total and dust $AOD_{550}$ data from the GOCART chemistry–aerosol-transport model simulations (version 006) are used in this study for the period 2000–2007. The GOCART model (see Chin et al., 2000, 2002, 2004, 2007; Ginoux et al., 2001, 2004) uses the assimilated meteorological fields of the Goddard Earth Observing System Data Assimilation System (GEOS DAS), which are generated by the Goddard Global Modeling and Assimilation Office (GMAO). The data that are used were acquired from an older version of NASA's GIOVANNI web database (http://disc.sci.gsfc.nasa.gov/giovanni/) and come from a simulation implemented at a spatial resolution of 2° (latitude) × 2.5° (longitude) with 30 vertical sigma layers (Chin et al., 2009). The model includes physicochemical processes of major tropospheric aerosol components (sulfates, dust, black carbon, organic carbon, sea salt) and precursor gases ($SO_2$ and dimethylsulfide), incorporating various atmospheric processes. The total $AOD_{550}$ from GOCART compared to ground-based observations from the AERONET exhibits a relative mean bias (mean(GOCART) / mean(AERONET)) of 1.120, 1.135 and 0.959 over Europe, northern Africa and for the whole globe, respectively.

### 2.8 Ancillary data

Apart from the main datasets presented above, three additional datasets were used in order to support our findings. OMI/AURA daily gridded (Bucsela et al., 2013) tropospheric $NO_2$ columnar data (OMNO2d version 2.1) at a spatial resolution of $0.25^\circ \times 0.25^\circ$ were acquired from NASA's GIOVANNI web database (http://giovanni.gsfc.nasa.gov/giovanni/) for the period 2005–2012. The quality-checked data used in this work correspond to sky conditions where the cloud fraction is less than 30 %. Planetary boundary layer (PBL) $SO_2$ daily gridded columnar data (OMSO2e version 1.1.7) were also acquired from GIOVANNI for the same period. The OMSO2e gridded data ($0.25^\circ \times 0.25^\circ$) used in this work are produced from best level-2 pixel data, screened for OMI row anomalies and other data quality flags. The PBL $SO_2$ column retrievals are produced with an algorithm based on principal component analysis (PCA) of the OMI radiance data (Li et al., 2013). Finally, monthly precipitation data from the 3B43 TRMM and Other Sources Monthly Rainfall Product (version 7) at a spatial resolution of $0.25^\circ \times 0.25^\circ$ for the period 2000–2012 were obtained from GIOVANNI. This dataset is derived from 3-hourly precipitation retrievals from the Precipitation Radar (PR), the TRMM Microwave Imager (TMI) and the Visible and Infrared Scanner (VIRS) aboard the TRMM (Tropical Rainfall Monitoring

Mission) satellite merged with other satellite-based precipitation data and the Global Precipitation Climatology Centre (GPCC) rain gauge analysis (Huffman et al., 2007).

## 3 Methodology

### 3.1 Compiling a MODIS 0.1° × 0.1° gridded dataset

To investigate the spatial and temporal variability of aerosols over the Eastern Mediterranean, we first created a $0.1^\circ \times 0.1^\circ$ daily gridded aerosol dataset using single-pixel level-2 $AOD_{550}$ and $FMR_{550}$ data from MODIS Collection 051. The same resolution has been utilized in previous studies (e.g., Barnaba and Gobbi, 2004) in the region, however, without reporting on the gridding methodology followed. In this work we present a gridding methodology that could be used as a reference for future regional studies. The methodology has been successfully applied in the past on level-2 MODIS Terra data in different cases studies, e.g., in order to examine the weekly cycle patterns of $AOD_{550}$ over the region of central Europe and the aerosol load changes observed over a cement plant in Greece due to changes in the deposition practices of the primary materials (see Georgoulias and Kourtidis, 2012; Georgoulias et al., 2012; Kourtidis et al., 2014). In the following lines we proceed to a detailed description of the method, underlining the potential of it being used in detailed quantitative studies like this one.

First, a $0.1^\circ \times 0.1^\circ$ resolution grid covering the Eastern Mediterranean (30–45° N, 17.5–37.5° E) is defined which corresponds to 30 000 grid cells. As already mentioned in Sect. 2.1, only level-2 single-pixel $AOD_{550}$ measurements with a QAC flag of 3 and a QAC flag greater than 0 were used over land and over sea, respectively, to ensure the high quality of the data. Pixels are attributed to a specific grid cell if their center falls within a $25 \times 25\,km^2$ square window around the grid cell (see Fig. S1 in the Supplement). These pixels are then used for the calculation of daily averages. As shown in Figure S1, a grid cell of 0.1° ($\sim 10$ km) is as big as the center of a large Mediterranean city like Thessaloniki, northern Greece ($\sim 1$ million inhabitants). The procedure was followed separately for MODIS Terra and Aqua data. In cases of grid cells with no DT MODIS observations, data from the DB algorithm were used (over bright arid and semi-arid regions of northern Africa), constituting only a small part of the gridded dataset.

The size of the gridding window was selected following Koukouli et al. (2007). They used both 10 and 25 km windows, showing that the latter allows for the inclusion of more data points without undermining the ability of monitoring the aerosol load over a specific spot accurately. In addition, in cases of urban sites, a window of 25 km allows for the inclusion of pixels from the surrounding non-urban surfaces where the MODIS surface reflectance parameterization is better (Levy et al., 2010). The size of each MODIS pixel is 10 km at nadir, but at the swath edges, it may become 2–3 times larger. Hence, ideally the maximum number of pixels that could be used in the daily averaging is nine. The overlap between the windows of neighboring grid cells does not affect the representativeness of the dataset over each grid cell. Aerosols are transported by air masses throughout the day, and thus the aerosol load in neighboring grid cells is not expected to be completely independent.

In order to make sure that the use of a 25 km gridding window is optimal for capturing local pollution sources we repeated the same procedure for bigger gridding windows (50, 75 and 100 km) using MODIS Terra $AOD_{550}$ data for the year 2004. Numerous aerosol hot spots cannot be seen as the gridding window becomes bigger and there is a significant smoothing of the aerosol patterns, mainly over land (Fig. S2). The use of the MODIS gridded dataset in the detection of local aerosol hot spots is discussed in more detail in Sect. 4. In addition, we conducted a detailed validation of the MODIS data against sun photometric data from a total of 13 AERONET stations in the region (see Fig. 1). The validation procedure was repeated several times for different spatial collocation windows, which were equal to the windows used for the gridding procedure (i.e., 25, 50, 75 and 100 km) and for different data quality criteria. The results of the validation procedure are presented in Sect. 4.1 while part of them is given in the Supplement of this paper (see Table S2 in the Supplement). Overall, it is shown that the gridding methodology followed here offers the best compromise for studying the spatial variability of aerosols on a regional or local scale, preserving, at the same time, the representativeness of the real aerosol load over each specific spot.

In order to generalize our results, nine different subregions (Fig. 1) were selected apart from the three basic regions of interest, namely, the whole Eastern Mediterranean (EMT) and the land (EML) and oceanic (EMO) areas of the region. The selection was done mainly taking geographical criteria, but also land type and land use criteria, into account. The four subregions that correspond to the land regions of the Eastern Mediterranean are the northern Balkans land (NBL), the southern Balkans land (SBL), the Anatolia land (ANL) and the northern Africa land (NAL) region, while the five subregions that correspond to the oceanic regions are the Black Sea oceanic (BSO), the northwestern oceanic (NWO), the southwestern oceanic (SWO), the northeastern oceanic (NEO) and the southeastern oceanic (SEO) region. Mean values of the total $AOD_{550}$ from the Terra and Aqua MODIS are reported for each one of the three basic regions of interest and their nine subregions in Sect. 4.

### 3.2 Contribution of different aerosol types to $AOD_{550}$

#### 3.2.1 Sea

In order to quantify the contribution of different types of aerosols to the total $AOD_{550}$ we followed a different ap-

**Table 1.** Full name, abbreviation, geolocation, host country and type of the 13 AERONET Cimel sun photometer sites used for the validation of MODIS Terra and Aqua Collection 051 observations. The common measurement period of MODIS and AERONET data and the corresponding overpass time of MODIS Terra and Aqua (italics) over each station are also given.

| AERONET station | Lat (° N) | Long (° E) | Period of study | Country | Type | TERRA overpass | *AQUA overpass* |
|---|---|---|---|---|---|---|---|
| ATHENS-NOA (ATH) | 37.988 | 23.775 | 05/2008–10/2012 | Greece | Urban (coastal) | 09:23 ± 22 min UT | *11:32 ± 22 min UT* |
| Bucharest Inoe (BUC) | 44.348 | 26.030 | 07/2007–09/2012 | Romania | Suburban (coastal) | 09:17 ± 24 min UT | *11:15 ± 20 min UT* |
| CUT-TEPAK (CUT) | 34.675 | 33.043 | 04/2010–12/2012 | Cyprus | Urban (coastal) | 08:43 ± 25 min UT | *10:55 ± 25 min UT* |
| Eforie (EFO) | 44.075 | 28.632 | 09/2009–12/2012 | Romania | Rural (coastal) | 09:09 ± 21 min UT | *11:04 ± 21 min UT* |
| FORTH Crete (FOR) | 35.333 | 25.282 | 01/2003–08/2011 | Greece | Rural (coastal) | 09:12 ± 24 min UT | *11:25 ± 25 min UT* |
| IMS-METU-ERDEMLI (IMS) | 36.565 | 34.255 | 01/2004–01/2012 | Turkey | Rural (coastal) | 08:39 ± 23 min UT | *10:48 ± 22 min UT* |
| Lecce University (LEC) | 40.335 | 18.111 | 03/2003–12/2012 | Italy | Suburban (coastal) | 09:44 ± 25min UT | *11:49 ± 25 min UT* |
| Nes ziona (NES) | 31.922 | 34.789 | 02/2000–12/2012 | Israel | Suburban (coastal) | 08:38 ± 24 min UT | *10:44 ± 25 min UT* |
| SEDE BOKER (SED) | 30.855 | 34.782 | 01/2000–04/2012 | Israel | Rural (semi-arid) | 08:30 ± 27 min UT | *10:50 ± 25 min UT* |
| Sevastopol (SEV) | 44.616 | 33.517 | 05/2006–12/2012 | Ukr. Crimea | Urban (coastal) | 08:51 ± 21 min UT | *10:40 ± 21 min UT* |
| Thessaloniki (THE) | 40.630 | 22.960 | 09/2005–12/2012 | Greece | Urban (coastal) | 09:28 ± 25 min UT | *11:32 ± 22 min UT* |
| TUBITAK UZAY Ankara (TUB) | 39.891 | 32.778 | 12/2009–04/2012 | Turkey | Urban (continental) | 08:48 ± 26 min UT | *10:56 ± 24 min UT* |
| Xanthi (XAN) | 41.147 | 24.919 | 01/2008–10/2010 | Greece | Rural (coastal) | 09:18 ± 25 min UT | *11:24 ± 21 min UT* |

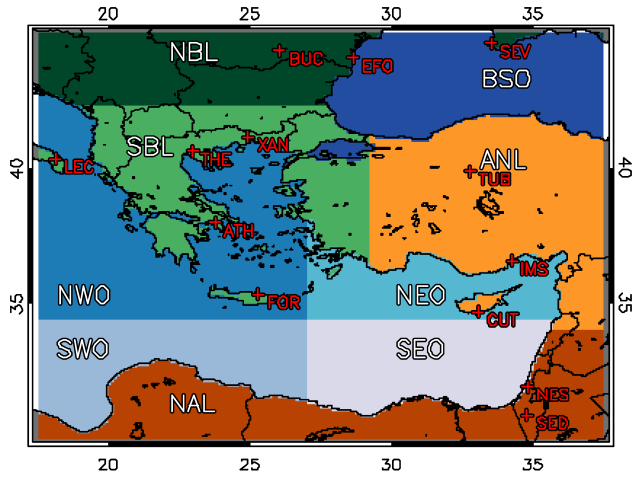


**Figure 1.** Eastern Mediterranean map with the nine subregions selected for the generalization of our results and the location of the AERONET stations used for the validation of MODIS satellite data. The nine subregions are NBL (northern Balkans land), SBL (southern Balkans land), ANL (Anatolia land), NAL (northern Africa land), BSO (Black Sea oceanic), NWO (northwestern oceanic), SWO (southwestern oceanic), NEO (northeastern oceanic) and SEO (southeastern oceanic). The full names and the geolocation of the 13 AERONET stations appearing in the map are available in Table 1.

proach for sea and land. This is due to the lack of reliable $FMR_{550}$ retrievals over land (e.g., see Levy et al., 2010; Georgoulias and Kourtidis, 2011), which are crucial for the algorithms used in this work. Over the sea we utilize wind speed data at 10 m above surface from the ERA-Interim reanalysis, AI data from TOMS and OMI, along with $AOD_{550}$ and $FMR_{550}$ from the MODIS Terra and Aqua gridded datasets presented above. All the datasets were brought to the same 0.1 degree spatial resolution as MODIS by using bilinear interpolation. In the case of TOMS and OMI we used monthly mean AI data following Bellouin et al. (2008) in order to avoid gaps, especially during the TOMS period.

In general, the algorithm used over the oceanic regions (see Fig. 2) is similar to the one presented in Bellouin et al. (2008). First, the marine $AOD_{550}$ ($\tau_m$) is calculated from near-surface wind speed using a linear relation that has been obtained from ground-based studies over pollution-free oceanic regions. Bellouin et al. (2008) use the linear relation of Smirnov (2003). Then, if $\tau_m$ is greater than or equal to $AOD_{550}$, it is assumed that there are marine particles only over this region. If $\tau_m$ is smaller than $AOD_{550}$, a decision tree is followed, which is first based on $FMR_{550}$ and then on AI in order to reach a conclusion about the type of aerosols that accounts for $AOD_{550}$. If $FMR_{550}$ is smaller than the critical value of 0.35 and AI is greater than or equal to a critical value, it is assumed that there are both marine aerosols ($\tau_m$) and dust ($\tau_d = AOD_{550} - \tau_m$), while if AI is smaller than this critical value, it is assumed that there are marine aerosols only. The AI critical value is equal

to 1 in Bellouin et al. (2008). If $FMR_{550}$ is greater than or equal to 0.83 it is assumed that there are both anthropogenic ($\tau_a = AOD_{550} - \tau_m$) and marine aerosols ($\tau_m$). In the case of having an $FMR_{550}$ equal to 0.35 or greater than 0.35 but smaller than 0.83 one has to take AI into consideration again. If AI is less than the critical value it is assumed that there are marine aerosols ($\tau_m$) only, while in the opposite occasion it is assumed that all three types of aerosols that can be defined over oceanic regions by this algorithm, namely, dust [$\tau_d = (1 - FMR_{550})\ (AOD_{550} - \tau_m)$], anthropogenic [$\tau_a = FMR_{550}(AOD_{550} - \tau_m)$] and marine aerosols ($\tau_m$) are present. One should keep in mind that all the biomass burning aerosols are classified as anthropogenic by this method.

In this work, we proceeded to a fine-tuning of the algorithm for the region of the Eastern Mediterranean. First, we applied the algorithm to MODIS Terra data using the same equations and critical values as in Bellouin et al. (2008). The results showed that the original Bellouin et al. (2008) method might be valid for global studies but for a "closed" sea like the Mediterranean the method leads to a large overestimation of sea salt AODs and therefore underestimation of dust and anthropogenic aerosol AODs. Indicative of this situation is Fig. S3 where we present the relative contribution of dust, marine and anthropogenic aerosols per month over the oceanic regions of the Eastern Mediterranean as calculated using the original Bellouin et al. (2008) method. It is shown that the marine contribution is several times higher than the values reported for the Mediterranean Basin in previous studies (e.g., see Nabat et al., 2012). Evaluation of the algorithm was done using dust $AOD_{532}$ data from the LIVAS CALIOP/CALIPSO product. From LIVAS we only use the high-quality Sahara dust product as a reference and not other aerosol type retrievals (e.g., marine aerosols) since the dust retrievals from CALIOP/CALIPSO are by far the most reliable (e.g., Burton et al., 2013). We performed several tests by changing the linear relation that connects $\tau_m$ with near-surface wind speed and the AI critical values, and we compared the dust $AOD_{550}$ seasonal variability with the LIVAS $AOD_{532}$ seasonal variability each time for the sea-covered subregions of the Eastern Mediterranean. Results from this algorithm-tuning procedure can be found in Fig. S4e–i where one can also see the underestimation of dust $AOD_{550}$ from the original Bellouin et al. (2008) algorithm.

The linear relation given in Kaufman et al. (2005) was finally selected ($\tau_m = 0.007\,ws + 0.02$). The 2000–2012 average wind speed over the sea for the region of the Eastern Mediterranean is $\sim 5.3\,m\,s^{-1}$. Kaufman et al. (2005) reduced the offset in the linear relation of Smirnov (2003) from 0.06 to 0.02 to fit the average baseline AOD of 0.06 for the typical wind speed of $6\,m\,s^{-1}$. In addition, our tests showed that an AI critical value of 1 performs well over the region of the Eastern Mediterranean. The results did not change significantly when using other AI thresholds (e.g., 0.5, which is suggested in Jones and Christopher, 2011), and therefore we decided to adopt 1 as the AI critical value. Another test, following the example of other studies (see Lehahn et al., 2010), was to assume that for wind speed less than $5\,m\,s^{-1}$, there is very little or no sea-spray particle production (limited bursting of entrained air bubbles associated with whitecap formation). In this case, $\tau_m$ is stable, equal to the offset of the linear relation between $\tau_m$ and wind speed, which is indicative of the background sea salt $AOD_{550}$. However, this test reveals that the effect of assuming stable $\tau_m$ for wind speed less than $5\,m\,s^{-1}$ is insignificant, and therefore we chose to follow the Kaufman et al. (2005) linear relationship for the whole wind speed range. As shown in Fig. S4e–i, the seasonal variability when applying our modified algorithm over oceanic regions is very close to the LIVAS dust $AOD_{532}$ especially for the months with lower dust load (June–January). It is also shown that dust AODs from this algorithm are closer to the LIVAS dust product than dust AODs are from MACC reanalysis do. The slight overestimation of dust AOD or the shift of the maximum dust load we observe for the period of high dust loads in the region (February–May) is probably connected to the narrow swath and the 16-day time period of CALIPSO, which means that several dust events might be not observed by the CALIOP instrument contrary to MODIS, which has a daily coverage.

### 3.2.2 Land

As already mentioned in the previous paragraph, a different approach is followed over the land regions of the Eastern Mediterranean due to the low confidence in the MODIS $FMR_{550}$ and Ångström exponent retrievals over land compared to that over ocean (e.g., see Levy et al., 2010; Georgoulias and Kourtidis, 2011). This limitation does not allow us to distinguish the contribution of fine- and coarse-mode aerosols in terms of $AOD_{550}$. In this case, we choose to use daily model fields of the dust contribution to the total AOD (here MACC reanalysis and GOCART). We follow a method similar to the one presented in Bellouin et al. (2013). Specifically, we calculate the dust $AOD_{550}$ by scaling the MODIS $AOD_{550}$ data with the MACC or GOCART dust / total $AOD_{550}$ ratios [$f_d = \tau_{d(model)}/\tau_{(model)}$] on a daily basis.

Since the MACC data are only available from 2003 to 2012, in order to take advantage of the full MODIS dataset (March 2000–December 2012), data from the GOCART model were used for the period 2000–2002. The GOCART data were normalized in order to be consistent with the MACC data. Daily dust / total $AOD_{550}$ ratios ($f_d$) from the common GOCART–MACC period 2003–2007 were first brought to a common $1^\circ \times 1^\circ$ spatial resolution using bilinear interpolation, and then we calculated the regression line for each grid cell on a seasonal basis. The linear relations were used afterwards in order to normalize the 2000–2002 GOCART ratios to have a homogeneous dataset. The slopes and offsets of these regression lines and the corre-

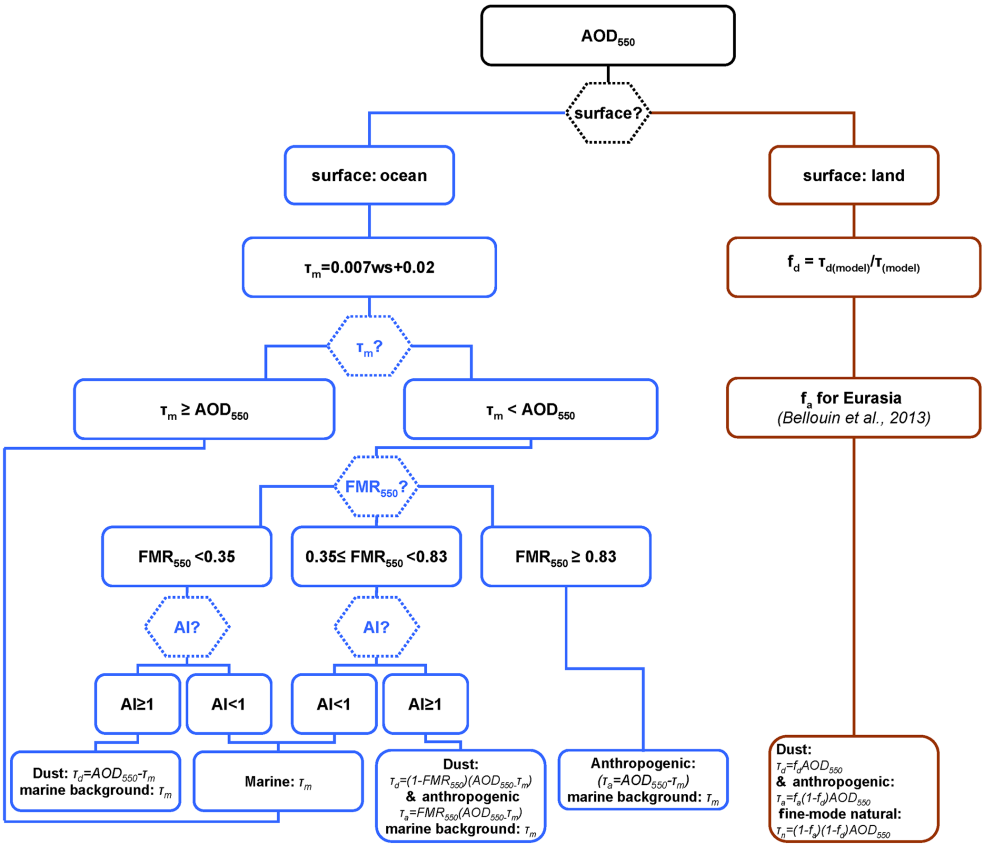


**Figure 2.** Flowchart with the methodology followed for the calculation of the anthropogenic aerosol, dust and marine aerosol optical depths ($\tau_a$, $\tau_d$ and $\tau_m$) over the sea (blue color) and the anthropogenic aerosol, dust and fine-mode natural aerosol optical depths ($\tau_a$, $\tau_d$ and $\tau_n$) over land (brown color).

sponding correlation coefficients ($R$) can be seen in Figs. S5, S6 and S7, respectively. Overall, for the whole time period, the MACC reanalysis $f_d$ ratios are lower by $\sim 26\,\%$ from the GOCART $f_d$ ratios, and the linear relation connecting the two products is $f_{dMACC} = 0.4964\, f_{dGOCART} + 0.0952$ with a correlation coefficient $R$ of 0.74. The $f_d$ values of the merged GOCART–MACC (2000–2012) time series were checked using the Standard Normalized Homogeneity Test (SNHT) as described in Alexandersson (1986). The statistical significance was checked following Khaliq and Ouarda (2007), and the $f_d$ time series were found to be homogeneous (see Fig. S8). Hence, this test verifies that the use of the merged GOCART–MACC $f_d$ dataset will not insert any artifacts (e.g., trends or breaks) in the algorithm. Finally, the $f_d$ data were brought to the same spatial resolution with MODIS data ($0.1^\circ \times 0.1^\circ$) using bilinear interpolation again.

After the calculation of $\tau_d$ with the use of $f_d$ values ($\tau_d = f_d AOD_{550}$), we proceed to the calculation of the anthropogenic contribution to the total $AOD_{550}$ ($\tau_a$) by multiplying the non-dust part of $AOD_{550}$ with the anthropogenic fraction $f_a$ for the region of Eurasia ($0.77 \pm 0.20$) given in Bellouin et al. (2013) ($\tau_a = f_a(1 - f_d)AOD_{550}$). The rest of the total $AOD_{550}$ is attributed to the fine-mode natural aerosols ($\tau_n = (1 - f_a)(1 - f_d)AOD_{550}$) (see Fig. 2). As discussed in Bellouin et al. (2013), the fine-mode natural aerosols consist of sea salt, dimethyl sulfide from land and oceanic sources, $SO_2$ from degassing volcanoes and secondary organic aerosols from biogenic emissions. It has to be highlighted that like in the case of oceanic regions, the biomass burning aerosols are classified as anthropogenic by this algorithm. As shown in Fig. S4a–d, the seasonal variability of $\tau_d$ over land-covered regions is very close to the LIVAS dust $AOD_{532}$ which is used as a reference.

Overall, the algorithm described above performs well as far as dust is concerned. This is further shown when comparing MODIS Terra and Aqua $\tau_d$ values with collocated AERONET observations for dust-dominated days (see Fig. S9). The method followed for the collocation of the data is similar to the one presented in Sect. 4.1, while dust-dominated days were days with an AERONET AE smaller than 1 (see Mateos et al., 2014) and a MODIS-based $\tau_d$ greater than $\tau_a$ and $\tau_n$ or $\tau_m$. The uncertainties of the calculated $\tau_a$, $\tau_d$, $\tau_n$ and $\tau_m$ values, which are inserted by the input data and the assumptions of the algorithm, are expected to be similar to the ones presented in Bellouin et al. (2013). Bellouin et al. (2013), using Monte Carlo analysis, indicated that

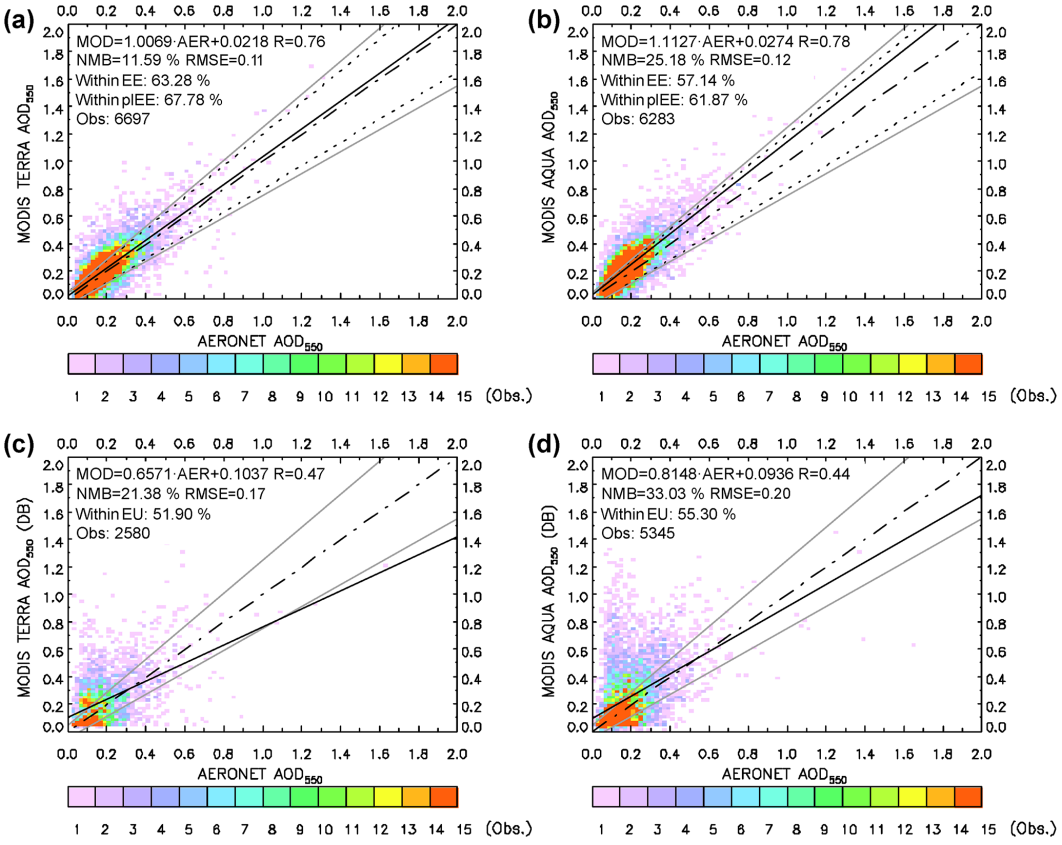


**Figure 3.** Comparison of spatially (using a $25 \times 25\,km^2$ window around each station) and temporally ($\pm 30$ min from the MODIS overpass time) collocated MODIS Collection 051 level-2 and AERONET sun photometric (quadratically interpolated) $AOD_{550}$ observations for the Eastern Mediterranean stations: **(a)** for MODIS Terra DT data, **(b)** for MODIS Aqua DT data, **(c)** for MODIS Terra DB data and **(d)** for MODIS Aqua DB data. The color scale corresponds to the number of MODIS–AERONET collocation points that fall within $0.02 \times 0.02$ grid boxes. The solid line is the regression line of the MODIS–AERONET observations, the dashed-dotted line is the 1 : 1 line, the dotted lines represent the expected error (EE) envelope and the gray lines the pre-launch expected error (plEE) envelope (expected uncertainty – EU envelope for DB data). The slope and the intercept of the regression line, the correlation coefficient $R$, the normalized mean bias (NMB), the root mean square error (RMSE), the percentage of the collocation points that fall within the EE and plEE and the number of all the collocation points are given on the plots.

$\tau_a$ can be specified with an uncertainty of $\sim 23\,\%$ over land and $\sim 16\,\%$ over the ocean, $\tau_d$ can be specified with an uncertainty of $\sim 19\,\%$ over land and $\sim 33\,\%$ over the ocean, $\tau_n$ can be specified with an uncertainty of $\sim 41\,\%$ and $\tau_m$ with an uncertainty of $\sim 28\,\%$. The results of the application of the algorithm described in the paragraphs above are presented in the following section (Sect. 4) by means of maps, pie charts, plots and tables for each one of the three basic regions of interest and their nine subregions.

## 4 Results and discussion

### 4.1 Validation of MODIS gridded data using ground-based observations

As discussed in Sects. 2 and 3, the high-quality (QAC: 3) DT level-2 Collection 051 MODIS data used in this work were validated in detail against data from 13 AERONET stations (see Fig. 1). The stations were selected to make sure that their version 2.0 level 2.0 high-quality cloud-screened Cimel sun photometric observations were covering at least 2 years and there were at least 100 common days of AERONET and MODIS observations. The exact geolocation of the AERONET stations is given in Table 1 (see also Fig. 1) along with the period of available data, the hosting country, the type of the station (e.g., urban/rural, coastal/continental) and the corresponding mean overpass time of Terra and Aqua MODIS. First, we spatially and temporally collocated the MODIS and AERONET observations by temporally averaging AERONET measurements within $\pm 30$ min from the MODIS overpass time (see Levy et al., 2010) and spatially averaging MODIS measurements centered within a $25 \times 25\,km^2$ window around each station (see Koukouli et al., 2010). The use of a collocation window equal

to the one used for the gridding procedure, practically allows us to validate the $0.1^\circ \times 0.1^\circ$ MODIS gridded product at the same time.

The regression lines between MODIS and AERONET AODs are shown in Fig. 3, while details about the validation results can be found in Table 2. Overall, the MODIS Terra DT Collection 051 data overestimate $AOD_{550}$ by 11.59 % (normalized mean bias – NMB), with 63.28 % of the data falling within the expected error (EE) envelope and 67.78 % within the pre-launch expected error (plEE) envelope. The expected error envelope is defined as $AOD - |EE| \leq AOD_{MODIS} \leq AOD + |EE|$, with EE being $\pm(0.05 + 0.15\,AOD)$ (Levy et al., 2010) and plEE being $\pm(0.05 + 0.20\,AOD)$ (Kaufman et al., 1997). On the other hand, the MODIS Aqua DT Collection 051 data overestimate $AOD_{550}$ by 25.18 % (NMB), with 57.14 % of the data falling within the EE envelope and 61.87 % within the plEE envelope. The percentage of the MODIS Terra and Aqua data falling within the EE envelope is close to the 57 % given in Remer et al. (2005) for the Eastern Mediterranean. The validation results can be found in Table S1 for each station separately. The results discussed in this paragraph are comparable to the ones appearing in previous studies focusing on the Mediterranean region (see Papadimas et al., 2009; Koukouli et al., 2010). In general, it is shown here that the MODIS Terra Collection 051 data exhibit a better agreement with the ground-based observations from AERONET than MODIS Aqua data do. Therefore, the statistics appearing for MODIS Terra throughout the paper could be considered more robust.

To be in line with the global validation of the DT Collection 051 product by Levy et al. (2010), we also performed a validation with the specifications used in their work. We used a $50 \times 50\,km^2$ window for the spatial collocation of the MODIS and AERONET data, while only days with at least five MODIS retrievals and two AERONET measurements were taken into account. The increased size of the collocation window improves the results of the validation. As shown in Table 2, MODIS Terra DT Collection 051 data overestimate $AOD_{550}$ by 5.10 % (NMB), with 70.17 % of the data falling within the EE envelope and 74.64 % within the plEE envelope. For MODIS Aqua, the NMB is 15.34 %, while the percentage of the measurements falling within the EE and plEE envelope is 66.76 and 70.45 %, respectively. These results for the Eastern Mediterranean are close to the global ones presented in Levy et al. (2010).

As discussed in Sect. 3.1, data from the DB algorithm were used over bright arid and semi-arid regions of northern Africa for the production of the $0.1^\circ \times 0.1^\circ$ MODIS gridded dataset for grid cells with no DT data. Therefore, in this work we also perform a validation of the DB Collection 051 product over the region of the Eastern Mediterranean. In the case of DB data, we first make use of all the available DB observations without any quality filtering over the 13 AERONET stations. A spatial window of 25–30 km has been typically used in the past for the collocation of MODIS DB data with the AERONET observations (see Shi et al., 2011; Ginoux et al.; 2012; Sayer et al., 2013, 2014), which is in line with the $25 \times 25\,km^2$ window used here. The MODIS Terra DB data overestimate $AOD_{550}$ by 21.38 % (NMB), with 51.90 % of the data falling within the expected uncertainty (EU) envelope, assuming a DB expected uncertainty of $\pm 0.05 \pm 20\,\%AOD_{AERONET}$ (Hsu et al., 2006). The MODIS Aqua DB Collection 051 data overestimate $AOD_{550}$ by 33.03 % (NMB), with 55.30 % of the data falling within the expected uncertainty envelope. We repeated the validation procedure for DB data, only taking the highest quality data into account. The sample of available measurements was diminished by a factor of 5 in the case of MODIS Terra and 6 in the case of MODIS Aqua, but the results were quite similar to the ones for the unfiltered data. Therefore, the use of unfiltered DB data during the gridding procedure does not insert any significant uncertainty. The DB results for the 13 AERONET stations examined here do not have the same agreement with the DT results and the ones presented in previous studies utilizing DB Collection 051 data for other stations and larger regions (see Shi et al., 2011; Ginoux et al., 2012). However, it has been reported that stations in the region (e.g., Sede Boqer in Israel) are among the ones with the greatest discrepancies between MODIS DB and AERONET measurements (Ginoux et al., 2012). Nevertheless, as commented in Sect. 3.1, the DB data constitute only a small fraction of the data used for the production of the MODIS gridded dataset (only $\sim 1$ % of the 30 000 grid cells covering the Eastern Mediterranean have only DB retrievals), and therefore they do not affect its quality significantly. Only areas in northern Africa are expected to be affected by the use of DB data due to the extended lack of DT data there.

As discussed in Sect. 3.1, the gridding procedure was repeated four times using a gridding window of 25, 50, 75 and 100 km using MODIS Terra $AOD_{550}$ data for the year 2004, showing that the 25 km window is optimal for capturing local pollution sources. In order to see how the size of the gridding window affects the agreement between MODIS and AERONET data, we also proceed to a validation of MODIS DT data against AERONET measurements using different spatial collocation windows (25, 50, 75 and 100 km) and two quality criteria, a "strict" one: at least two AERONET measurements for each MODIS–AERONET pair and a "stricter" one: at least five MODIS retrievals and two AERONET measurements for each MODIS–AERONET pair, as in Levy et al. (2010). The results for the DT MODIS Terra and Aqua data are presented in Table S2. In general, it is shown that the increased size of the spatial collocation window leads to an improvement of the bias between satellite- and ground-based observations. This is probably due to the inclusion of more observations into the calculations, which diminishes the noise of the MODIS observations. In addition, as expected, the stricter quality criteria lead to a better agreement between MODIS DT and AERONET data. Not only taking the NMB into account, but also the regression lines and the

**Table 2.** Results of the comparison of spatially (using a spatial window around each station) and temporally (±30 min from the MODIS overpass time) collocated MODIS Terra and Aqua (italics) Collection 051 level-2 and AERONET sun photometric (quadratically interpolated) $AOD_{550}$ observations for the Eastern Mediterranean stations. The algorithms used for the production of the validated MODIS data (DT and DB), the spatial window used for the spatial collocation ($25 \times 25\,km^2$ or $50 \times 50\,km^2$ window around each station) with the AERONET data, the average MODIS and AERONET $AOD_{550}$ and the corresponding $\pm 1\sigma$ values, the mean difference between them, the normalized mean bias (NMB) and the corresponding root mean square error (RMSE), the percentage of the collocation points that fall within the expected error (EE) envelope and the pre-launch expected error (plEE) envelope (expected uncertainty – EU envelope for DB data), the correlation coefficient $R$, the slope (a) and the intercept of the regression line (b) and the number of the collocation points are given in the table. L10 denotes the use of a collocation window of 50° × 50° as in Levy et al. (2010), while HQ denotes the use of high-quality data only.

| Alg. | Window | MODIS TERRA *MODIS AQUA* | AERONET | Mean diff. | NMB % | RMSE | In EE % | In plEE % | $R$ | $a$ | $b$ | Obs |
|---|---|---|---|---|---|---|---|---|---|---|---|---|
| DT | 25 km | $0.223 \pm 0.163$ | $0.200 \pm 0.123$ | $0.023 \pm 0.106$ | 11.59 | 0.11 | 63.28 | 67.78 | 0.76 | 1.007 | 0.022 | 6697 |
| *DT* | *25* km | *0.247 ± 0.173* | *0.197 ± 0.121* | *0.050 ± 0.109* | *25.18* | *0.12* | *57.14* | *61.87* | *0.78* | *1.113* | *0.027* | *6283* |
| DT | 50 $km_{(L10)}$ | $0.204 \pm 0.152$ | $0.194 \pm 0.124$ | $0.010 \pm 0.085$ | 5.10 | 0.09 | 70.17 | 74.64 | 0.83 | 1.016 | 0.007 | 6054 |
| *DT* | *50* $km_{(L10)}$ | *0.224 ± 0.155* | *0.194 ± 0.125* | *0.030 ± 0.088* | *15.34* | *0.09* | *66.76* | *70.45* | *0.82* | *1.018* | *0.026* | *5557* |
| DB | 25 km | $0.226 \pm 0.177$ | $0.186 \pm 0.128$ | $0.040 \pm 0.162$ | 21.38 | 0.17 | – | 51.90 | 0.47 | 0.657 | 0.104 | 2580 |
| *DB* | *25* km | *0.242 ± 0.217* | *0.182 ± 0.118* | *0.06 ± 0.196* | *33.03* | *0.20* | – | *55.30* | *0.44* | *0.815* | *0.094* | *5345* |
| $DB_{HQ}$ | 25 km | $0.229 \pm 0.158$ | $0.186 \pm 0.132$ | $0.043 \pm 0.141$ | 22.82 | 0.15 | – | 52.41 | 0.54 | 0.651 | 0.108 | 498 |
| *$DB_{HQ}$* | *25* km | *0.260 ± 0.220* | *0.186 ± 0.138* | *0.074 ± 0.204* | *39.84* | *0.22* | – | *52.34* | *0.42* | *0.670* | *0.136* | *896* |

other metrics appearing in Table S2, it is concluded that the 50 km window is the best choice for the validation procedure in line with Ichoku et al. (2002). On the other hand, the 25 km validation results are close to the 50 km ones (see Table S2), and at the same time the 25 km gridding window allows for a more efficient detection of local aerosol sources as shown in Sect. 3.1. Taking this into account, we suggest that the 25 km window used for the production of the 0.1° × 0.1° gridded MODIS dataset is the optimal selection for studying the spatial variability of aerosols, preserving, at the same time, the representativeness of the real aerosol load over each specific spot.

### 4.2 Aerosol spatial variability and hot spots

The $AOD_{550}$ spatial variability over the greater Eastern Mediterranean region for the period 2000–2012 as seen from the Terra MODIS 0.1° × 0.1° dataset is presented in Fig. 4. Several aerosol hot spots that coincide with megacities (e.g., Cairo, Istanbul), large cities (e.g., Athens, Ankara, Alexandria, Izmir, Thessaloniki) or even medium-sized cities (e.g., Larissa, Limassol), industrial zones (e.g., OSTIM Industrial Zone in Ankara, Turkey), power plant complexes (e.g., Maritsa Iztok complex in the Stara Zagora province in Bulgaria, Ptolemaida–Kozani power plants in western Macedonia, Greece), river basins (e.g., Evros River basin at the borders between Greece and Turkey), etc., can be detected on the map. Indicatively, in Fig. 4 we give a list of 35 local particle pollution sources in the region; however, careful inspection of this map and the seasonal maps presented in Fig. 6 allows for the detection of many more aerosol sources. The results from the analysis of Aqua MODIS data are pretty similar as shown in Fig. S10. A significant number of the local aerosol sources can also be detected on the OMI 2004–2012 tropospheric $NO_2$ and PBL $SO_2$ maps given in Fig. 5a and b, which reveal the origin of aerosols over these regions (e.g., traffic, industrial activities). However, there are regions of high aerosol load that cannot be seen in Fig. 5a and b and vice versa, which is indicative of the significant role of other anthropogenic or natural processes that contribute to the local aerosol load (e.g., fires, soil dust from agricultural activities or arid regions, Sahara dust transport).

The topography (Fig. 5c) and precipitation (see Fig. 5d for annual precipitation levels for the period 2000–2012 from TRMM) are also major determinants of the local $AOD_{550}$ levels. For example, regions with mountain ranges in the Balkan Peninsula (e.g., Pindus mountain range in Greece, Dinaric Alps that run through Albania and the former Yugoslav republics, the Balkan mountain range in central Bulgaria) are characterized by low AODs (see Fig. 4). In contrast, regions of low altitude are generally characterized by higher AODs because the majority of anthropogenic activities is usually concentrated there. In addition, low-altitude regions surrounded by high mountains are characterized by higher AODs as aerosols cannot be easily transported by the wind (e.g., the industrialized regions in central Bulgaria, which are confined between the high Balkan and Rodopi mountain ranges). As precipitation is the major removal mechanism of pollutants in the atmosphere, regions with high $AOD_{550}$ are, in many cases, connected to low precipitation levels and vice versa (see Figs. 4 and 5d). It has to be highlighted that the $AOD_{550}$ over these regions is high primarily due to the emissions and the atmospheric processes forming aerosol particles. The low removal rates from precipitation just preserve the $AOD_{550}$ levels high. A striking example is the region of Anatolia in central Turkey, which is characterized by lower precipitation levels and higher aerosol loads compared to the surrounding regions. Additionally, the low precipitation levels are partly responsible for the high aerosol loads appearing over northern Africa.

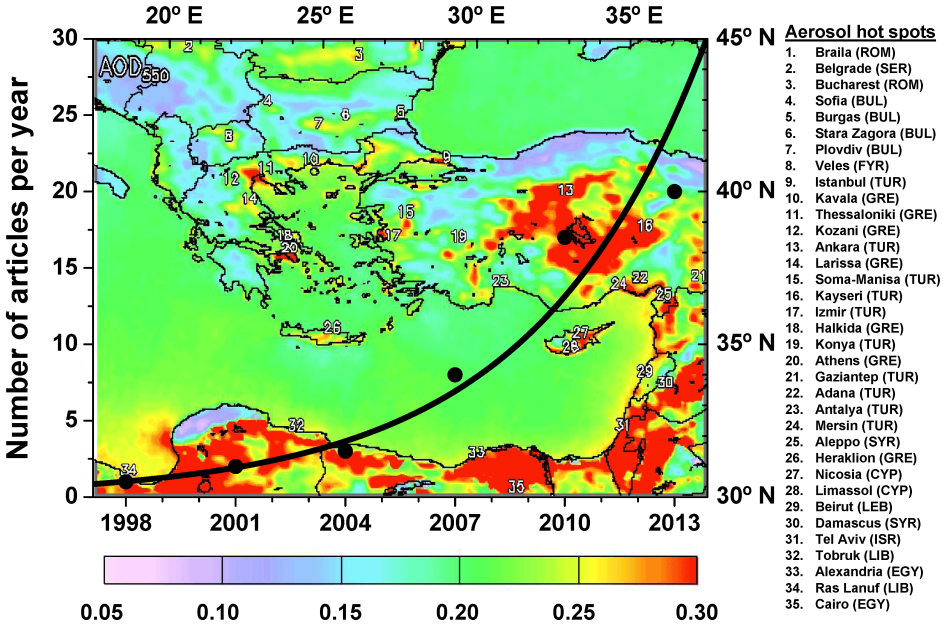


**Figure 4.** $AOD_{550}$ patterns over the Eastern Mediterranean as seen by MODIS Terra during the period March 2000–December 2012 (March 2000–December 2007 for regions of northern Africa covered by DB data only). The color scale corresponds to the $AOD_{550}$ levels, while the top $x$ axis and the right $y$ axis correspond to the longitude (° E) and latitude (° N), respectively. The position of 35 aerosol hot spots is marked on the map (numbers from 1 to 35), while the names of the places and the countries where the hot spots are located appear on the right of the map. In the same figure, the exponential growth of the number of satellite-based articles focusing on aerosols over the greater Eastern Mediterranean from 1997 to 2014 is shown (black line). The black dots represent the number of articles published within 3-year intervals. The bottom $x$ axis and the left $y$ axis correspond to the years and the number of published articles, respectively. The exponential growth corresponds to a near doubling of the publication rate every 3 years.

**Table 3.** $AOD_{550}$ levels, the corresponding $\pm 1\sigma$ values and the number of gridded values used for the calculations over the Eastern Mediterranean (EMT), over the land-covered part (EML), over the oceanic part and over the nine subregions of the Eastern Mediterranean appearing in Fig. 1 based on the MODIS Terra and Aqua (italics) observations.

| Region | MODIS TERRA $AOD_{550}$ | No. of values | *MODIS AQUA $AOD_{550}$* | *No. of values* |
|---|---|---|---|---|
| EMT | $0.215 \pm 0.187$ | 61 496 654 | *$0.217 \pm 0.199$* | *49 522 934* |
| EML | $0.219 \pm 0.165$ | 25 923 766 | *$0.239 \pm 0.189$* | *21 008 713* |
| EMO | $0.213 \pm 0.201$ | 35 572 888 | *$0.202 \pm 0.205$* | *28 514 221* |
| NBL | $0.183 \pm 0.163$ | 5 563 495 | *$0.187 \pm 0.162$* | *3 853 688* |
| SBL | $0.197 \pm 0.152$ | 7 345 829 | *$0.207 \pm 0.152$* | *5 272 449* |
| ANL | $0.223 \pm 0.146$ | 7 948 817 | *$0.228 \pm 0.148$* | *5 539 261* |
| NAL | $0.282 \pm 0.192$ | 5 065 625 | *$0.306 \pm 0.238$* | *6 343 315* |
| BSO | $0.198 \pm 0.150$ | 6 433 951 | *$0.183 \pm 0.134$* | *5 262 438* |
| NWO | $0.209 \pm 0.162$ | 11 645 069 | *$0.197 \pm 0.154$* | *9 231 630* |
| SWO | $0.226 \pm 0.266$ | 6 202 893 | *$0.223 \pm 0.310$* | *4 925 665* |
| NEO | $0.214 \pm 0.196$ | 4 807 910 | *$0.199 \pm 0.166$* | *3 896 554* |
| SEO | $0.221 \pm 0.236$ | 6 483 065 | *$0.210 \pm 0.239$* | *5 197 934* |

Overall, the mean $AOD_{550}$ for the whole period of interest is estimated at $0.215 \pm 0.187$ for Terra and $0.217 \pm 0.199$ for Aqua MODIS for the Eastern Mediterranean region, which is $\sim 45\,\%$ higher than the global average appearing in recent studies (e.g., Kourtidis et al., 2015). Over land, higher mean AODs are generally recorded ($0.219 \pm 0.165$ for Terra and $0.239 \pm 0.189$ for Aqua MODIS) than over the sea ($0.213 \pm 0.201$ for Terra and $0.202 \pm 0.205$ for Aqua MODIS). All these values, along with the mean AODs for the nine subregions of interest covering the Eastern Mediterranean, can be found in Table 3.

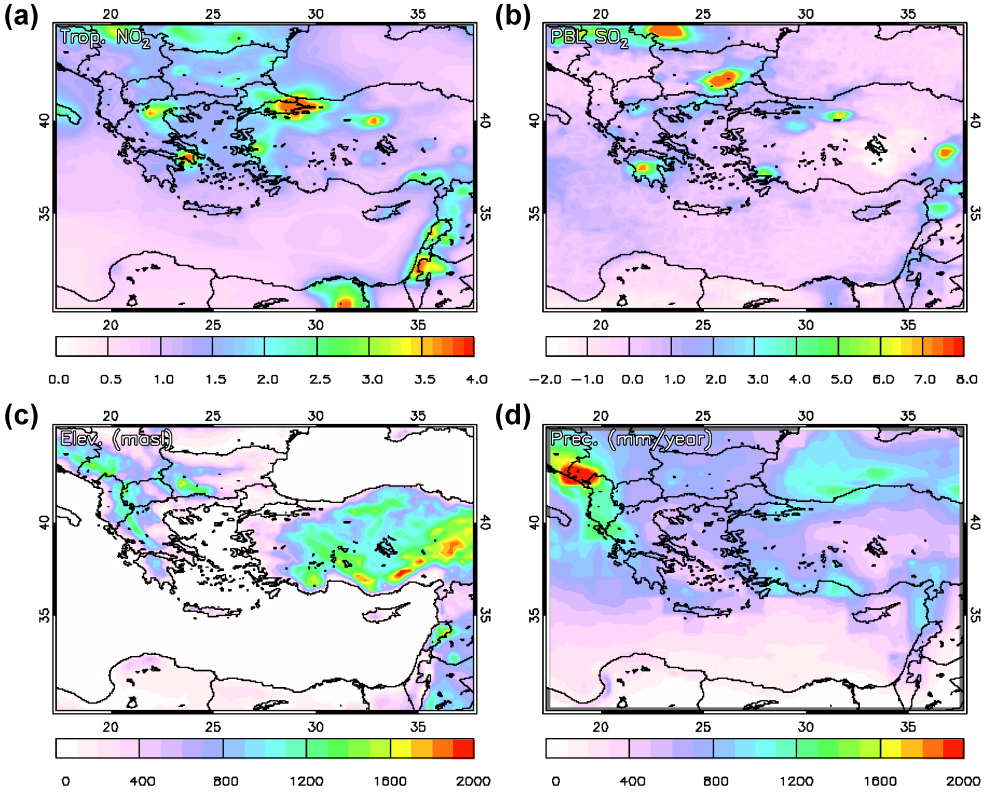


**Figure 5. (a)** Tropospheric $NO_2$ levels and **(b)** planetary boundary layer $SO_2$ levels (in $10^{15}$ molecules $cm^{-2}$) over the Eastern Mediterranean as seen from OMI/AURA (2005–2012), **(c)** topography (GTOPO elevation data in meters above sea level) and **(d)** annual precipitation levels (in mm $yr^{-1}$) from 3B43 TRMM and Other Sources Monthly Rainfall Product (2000–2012).

The $AOD_{550}$ spatial variability on a seasonal basis from MODIS Terra and Aqua is presented in Fig. 6 along with the difference between the two products. The majority of the local aerosol sources over land are more prominent in summer. The limited washout by precipitation (see also Papadimas et al., 2008) and also the enhanced photochemical production of secondary organic aerosols (Kanakidou et al., 2011 and references therein) contribute to the high AODs appearing over local sources. In addition, during summer, over the region, there is typically a significant transport of aerosols (e.g., see Kanakidou et al., 2011 and references therein) and gaseous pollutants like $SO_2$ and $NO_2$ (see Georgoulias et al., 2009; Zyrichidou et al., 2009) and biomass burning aerosols from central-eastern Europe. Over the sea, a profound maximum is observed in spring, extending across the northern African coast and the neighboring oceanic areas, which is due to the well-documented transport of significant amounts of dust from the Sahara (see Barnaba and Gobbi, 2004, and the list of references given in the Introduction). The seasonal variability of aerosols and the relative role of different aerosol types and various processes are discussed in more detail in Sect. 4.4.

The difference between MODIS Terra and Aqua Collection 051 $AOD_{550}$ over the Eastern Mediterranean is −0.002 (−1.40 %) for winter, −0.009 (−3.27 %) for spring, −0.011 (−4.46 %) for summer and 0.008 (4.40 %) for autumn. $AOD_{550}$ levels from Terra MODIS are lower than those from Aqua MODIS over land for all seasons. Over the sea, Terra MODIS $AOD_{550}$ levels are lower than that of Aqua MODIS only in winter. The fact that Terra MODIS measurements are systematically higher than that from Aqua over the sea by ∼ 0.01 on an annual basis is in line with the findings of previous global studies for Collection 5 (e.g., Remer et al., 2006, 2008). Locally, one can see regions with positive and negative differences between Terra and Aqua MODIS $AOD_{550}$. The patterns of the Terra–Aqua difference per season are presented in Fig. 6c, f, i and l, while the patterns of the percent difference are given in Fig. S11. The largest part of the Terra–Aqua MODIS differences over land and sea that are observed here may be attributed to the known calibration and sensor degradation issues of MODIS (for details see Levy et al., 2010, 2013; Lyapustin et al., 2014; Georgoulias et al., 2016). A significant effort has been undertaken to address these issues in the new (Collection 6) MODIS product (e.g., Levy et al., 2013; Lyapustin et al., 2014; Georgoulias et al., 2016), and a repetition of similar analysis with Collection 6 data in the future would be a valuable contribution. Taking the aforementioned issues and the retrieval

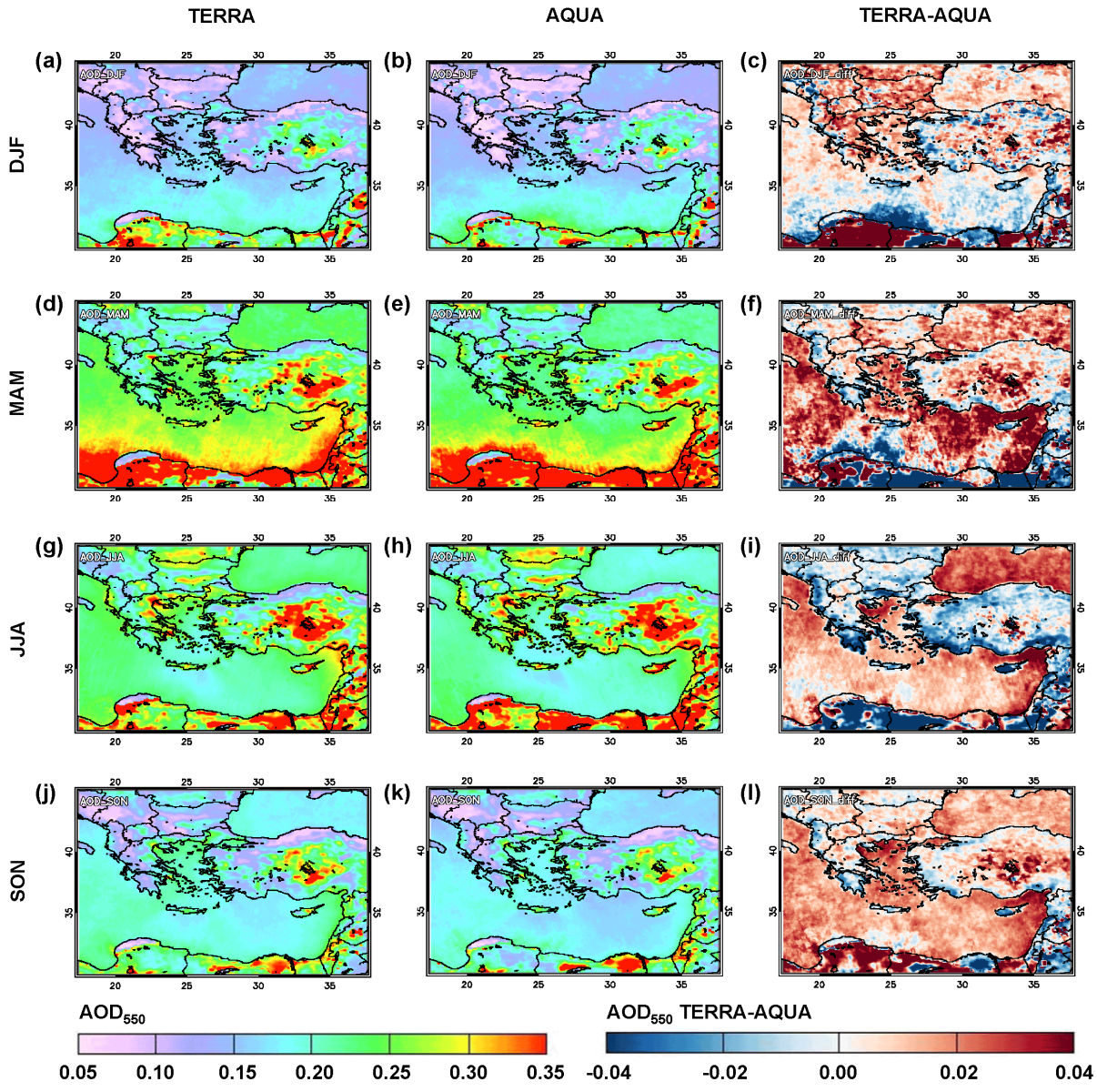


**Figure 6.** Seasonal $AOD_{550}$ patterns over the Eastern Mediterranean as seen by MODIS Terra (left column) during the period March 2000–December 2012 (March 2000–December 2007 for regions of northern Africa covered by DB data only) and MODIS Aqua (middle column) during the period July 2002–December 2012. The differences between MODIS Terra and Aqua $AOD_{550}$ on a seasonal basis appear in the right column.

uncertainty of MODIS into account, it becomes more than obvious that the attribution of observed differences between Terra and Aqua to the diurnal variability of aerosol load (e.g., over biomass burning regions) in the region is a difficult task. It is shown in Fig. S12 that the diurnal variability of $AOD_{550}$ from AERONET ranges significantly from station to station. The average hourly departure from the daily mean for the total of the 13 stations ranges from $\sim -5$ to $\sim 5$ %. Specifically, for the MODIS Terra and Aqua overpass times, the AERONET $AOD_{550}$ difference ranges from $\sim -10$ to $\sim 10$ % (see Fig. S12b). The Terra–Aqua $AOD_{550}$ difference is negative for the total of the 13 stations ranging from $\sim -25$ to $\sim -5$ %. It is shown in Fig. S12b that the two differences exhibit a similar variability from station to station, which indicates that part of the observed Terra–Aqua difference is indeed due to the diurnal variability of aerosols. However, as mentioned above, the diurnal variability of aerosols is a very delicate issue and should be comprehensively addressed in a future study. The same stands for other kind of variabilities, which could be connected to local and regional anthro-

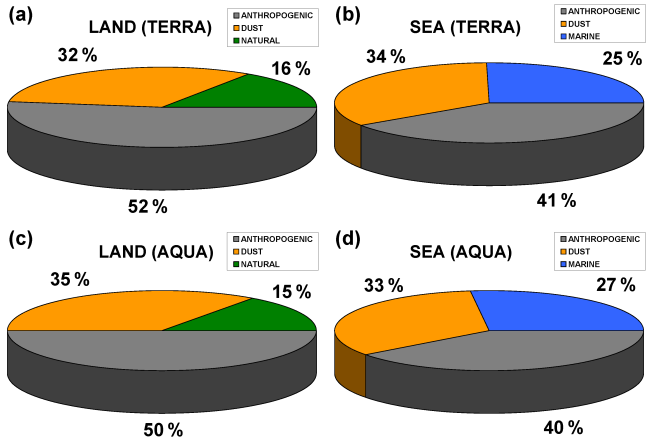


**Figure 7.** Relative contribution of anthropogenic aerosols, dust and fine-mode natural aerosols to the total $AOD_{550}$ over the land-covered part of the Eastern Mediterranean based on MODIS Terra **(a)** and MODIS Aqua **(c)** observations and relative contribution of anthropogenic aerosols, dust and marine aerosols to the total $AOD_{550}$ over the oceanic part of the Eastern Mediterranean based on MODIS Terra **(b)** and MODIS Aqua **(d)** observations.

pogenic activities like, e.g., the weekly cycle of aerosols (see Georgoulias and Kourtidis, 2011; Georgoulias et al., 2015).

### 4.3 Contribution of different aerosol types to the total $AOD_{550}$

#### 4.3.1 Annual contribution

As mentioned above, in our work we attempt to estimate the contribution of different aerosol types to the total $AOD_{550}$ over the region of the Eastern Mediterranean; this was calculated following the methodology presented in Sect. 3.2. For the land-covered areas, based on MODIS Terra observations, we estimate that 52 % ($0.112 \pm 0.087$) of the total $AOD_{550}$ is due to anthropogenic aerosols, 32 % ($0.074 \pm 0.080$) due to dust and 16 % ($0.034 \pm 0.026$) due to fine-mode natural aerosols (see Fig. 7). For the oceanic areas, 41 % ($0.086 \pm 0.085$) of the total $AOD_{550}$ is due to anthropogenic aerosols, 34 % ($0.076 \pm 0.185$) due to dust and 25 % ($0.054 \pm 0.018$) due to marine aerosols (see Fig. 7). The results based on observations from MODIS Aqua are similar. Over land, 50 % ($0.117 \pm 0.093$) of the total $AOD_{550}$ is anthropogenic, 35 % ($0.090 \pm 0.102$) is due to dust and 15 % ($0.035 \pm 0.028$) due to fine-mode natural aerosols, while, over the sea, 40 % ($0.079 \pm 0.080$) of the total $AOD_{550}$ is of anthropogenic origin, 33 % ($0.070 \pm 0.181$) is due to dust and 27 % ($0.054 \pm 0.018$) due to marine aerosols (see Fig. 7). These results, along with the relative contributions and the annual $\tau_a$, $\tau_d$, $\tau_n$ and $\tau_m$ levels for each one of the nine subregions of interest (see Fig. 1), are given in Table 4.

For anthropogenic aerosols, the region with the highest relative contribution is NBL (59 % for both Terra and Aqua MODIS), while the region with the lowest relative contribution is SWO (32 % for both Terra and Aqua MODIS) (see also Table 4). The spatial variability of $\tau_\alpha$ is presented in Fig. 8a for Terra MODIS and Fig. S13a for Aqua MODIS, the patterns being similar in both cases. Over land, the annual $\tau_a$ patterns are similar to the $AOD_{550}$ patterns, the highest values appearing over local particle pollution sources (cities, industrial zones, etc.). Over the sea, $\tau_a$ is higher along the coasts, while it drops significantly towards other directions. An interesting feature here is that the oceanic region of Black Sea (BSO) presents higher relative anthropogenic contributions than the rest of the oceanic subregions but also than land areas with significant anthropogenic sources (e.g., ANL and NAL). This is indicative of the transport of atmospheric particles from central Europe and biomass burning aerosols during the biomass burning seasons in April–May from Russia (across the latitudinal zone 45–55° N) and July–August from southwestern Russia and eastern Europe (Amiridis et al., 2010). These aerosols are transported at much lower latitudes as shown in previous studies (e.g., Vrekoussis et al., 2005; Karnieli et al., 2009), reaching the Sahara and the Middle East regions (Pozzer et al., 2015). The fact that $\tau_a$ drops gradually from the coasts is also seen in Fig. 9 where the latitudinal variability of the optical depths of the different aerosol types ($\tau_a$, $\tau_d$, $\tau_n$ and $\tau_m$) is presented for four bands that cover the whole Eastern Mediterranean. An interesting feature is that $\tau_a$ increases nearby the shoreline (particularly along the northern African coastal zone) before it gradually decreases. Over land aerosols are located within the atmospheric boundary layer, close to the emission sources, and hence their deposition and removal from the atmosphere is more efficient than over the sea. The particles, which are transported over the sea on the other hand, usually reach greater heights, which prolongs their lifetime.

As shown in Fig. 9, the same feature is observed for dust. Indicatively, $\tau_d$ and the relative contribution of dust to the total $AOD_{550}$ on an annual basis over the oceanic regions of SWO and SEO are, in general, higher than or comparable to the ones over NAL (see Table 4 for more details). In Fig. 9, the MODIS-based $\tau_d$ latitudinal variability is presented along with the latitudinal variability of dust $AOD_{532}$ and extinction coefficients of dust at 532 nm from LIVAS. As expected, in all cases $\tau_d$ decreases with distance from the large dust sources in the south and southeast (Sahara and the Middle East), with local maxima over the latitudinal zone from 35 to 40° N (especially for band 2 and band 3). The latitudinal variability of $\tau_d$ is similar to the latitudinal variability of dust $AOD_{532}$ for all the four bands, despite the fact that the MODIS-based data have a resolution 100 times higher (0.1° vs. 1°) and therefore are more sensitive to local characteristics. Dust reaches heights up to ~ 4–5 km in the area; however, the largest fraction of dust mass is confined within the first 2–3 km of the troposphere (see Fig. 9). The annual $\tau_d$ patterns are shown in Fig. 8b for Terra MODIS (Fig. S13b for Aqua MODIS). The main dust transport pathways over

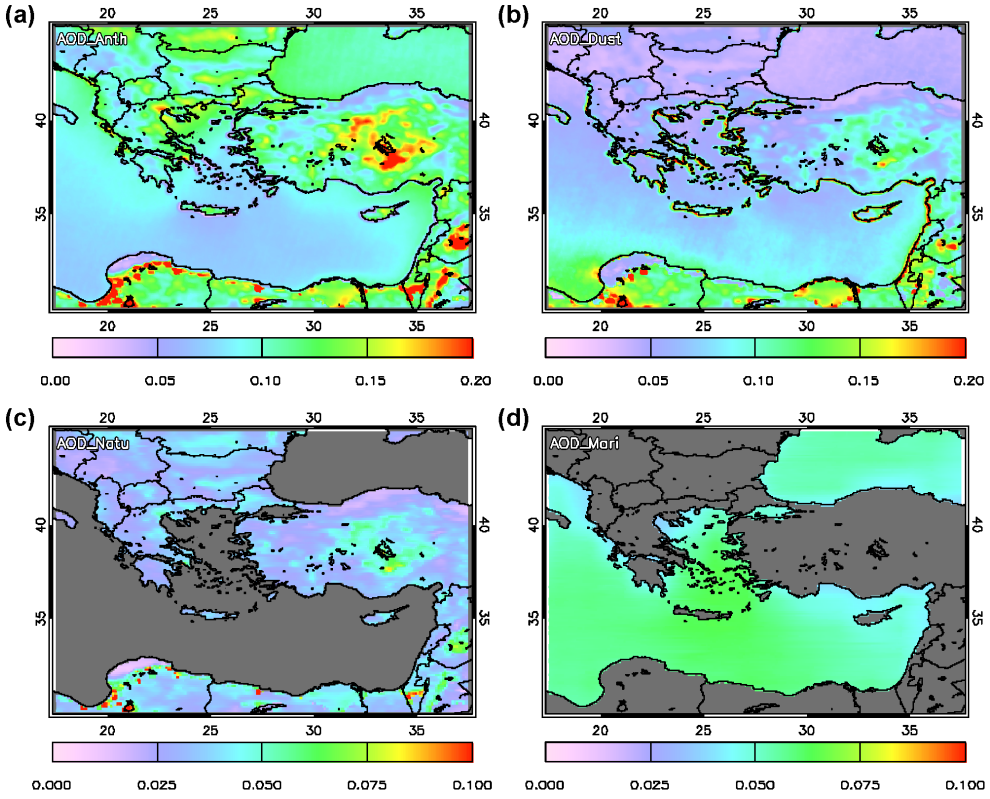


**Figure 8.** **(a)** Anthropogenic aerosol ($\tau_a$), **(b)** dust ($\tau_d$), **(c)** fine-mode natural aerosol ($\tau_n$) and **(d)** marine aerosol ($\tau_m$) patterns over the Eastern Mediterranean based on MODIS Terra observations during the period March 2000–December 2012 (March 2000–December 2007 for regions of northern Africa covered by DB data only).

the oceanic areas of the Eastern Mediterranean can be seen along with various local maxima over land. The highest $\tau_d$ values over land appear over the regions of NAL and ANL (see Table 4) and along the coasts. The high dust concentrations appearing over these regions are not only due to the transport of dust from the nearby deserts but also due to local dust sources. A recent study by Liora et al. (2015) reports various local sources of wind-blown dust along the coastal regions of Greece and Turkey, over the region of Anatolia in Turkey, over the Greek islands, Crete and Cyprus, and regions close to the coastal zone of Middle East. Their results are in good agreement with the $\tau_d$ patterns presented in this work.

As shown in Fig. 7, fine-mode natural aerosols exhibit the lowest contribution to the total $AOD_{550}$ compared to the other aerosol types over land. The spatial variability of $\tau_n$ is very low compared to $\tau_a$ and $\tau_d$ as shown in Figs. 8c and 9. It is inferred from the values appearing in Table 4 that $\tau_n$ increases slightly as one moves from north to south; however, the relative contribution of fine-mode natural aerosols to the total $AOD_{550}$ slightly decreases (i.e., 17.67 % over NBL and 14.97 % over NAL according to Terra MODIS observations). The latitudinal variability and the percentages appearing in Table 4 are in accordance with the relative contributions of biogenic aerosols to the total $AOD_{550}$ appearing over the Eastern Mediterranean in a recent modeling study (Rea et al., 2015).

Similar to fine-mode natural aerosols over land, marine aerosols generally have the lowest contribution to the total $AOD_{550}$ compared to the other aerosol types over the sea (see Fig. 7 and Table 4), except for BSO. The variability of $\tau_m$ is very low compared to $\tau_a$ and $\tau_d$. On an annual basis, high $\tau_m$ values appear over the Aegean Sea and the oceanic area between Crete and the northern African coast, while slightly lower values appear along the coasts of the Eastern Mediterranean (see Figs. 8d and 9). The $\tau_m$ patterns follow the near-surface wind speed patterns in the region (see Fig. S14), being in accordance with the $\tau_m$, marine particulate matter concentration or sea salt emission patterns appearing in other studies (Im et al., 2012; Nabat et al., 2013; Rea et al., 2015; Liora et al., 2015).

### 4.3.2 Seasonal contribution

The contribution of different aerosol types to the total $AOD_{550}$ over the Eastern Mediterranean varies from season to season. The relative contribution of each aerosol type over EML and EMO for each season is shown in Fig. 10. Over land, the relative contribution of $\tau_a$, $\tau_d$ and $\tau_n$ to the to-

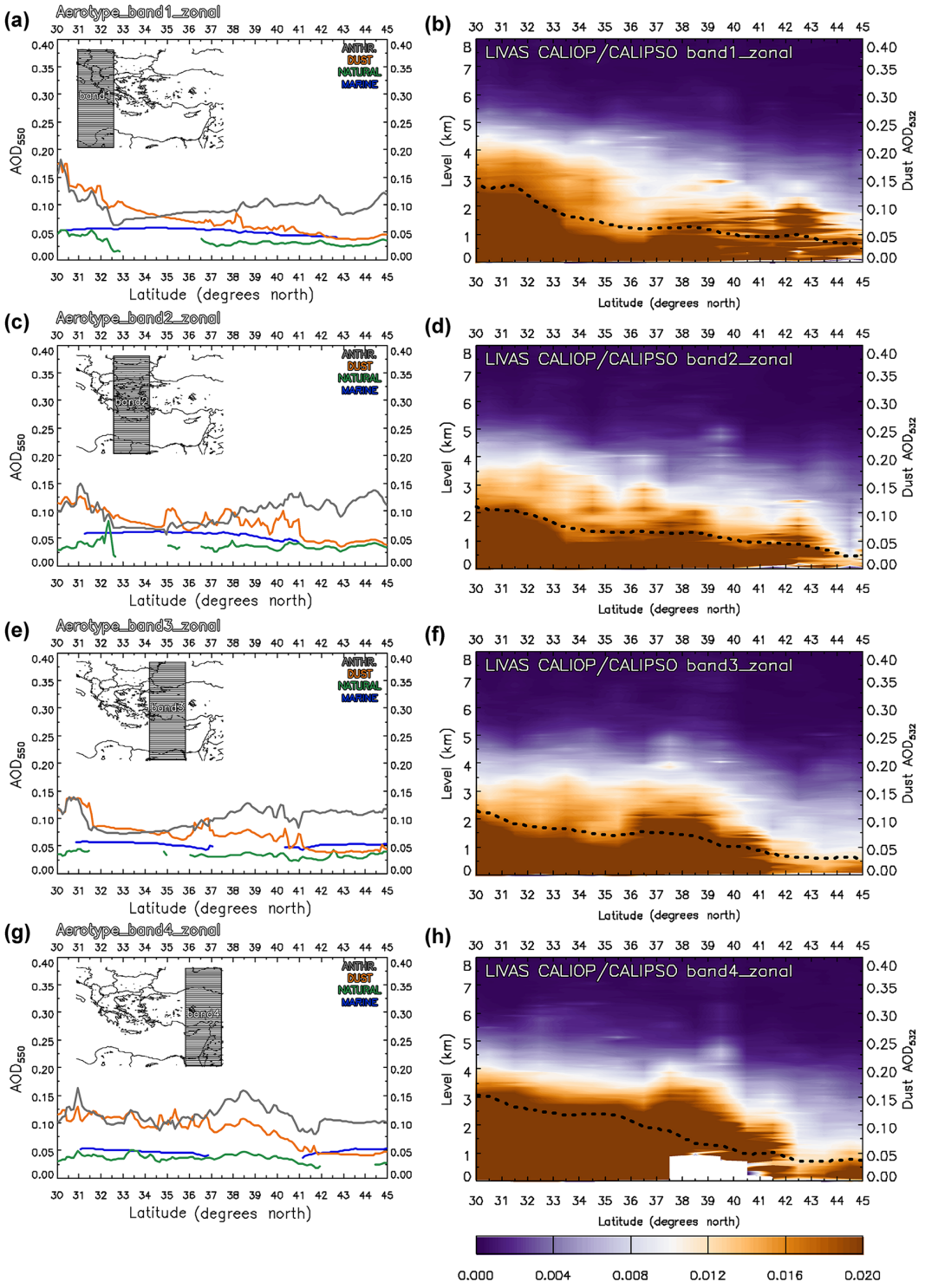


**Figure 9.** Left column: latitudinal variability of anthropogenic aerosols ($\tau_a$), dust ($\tau_d$), fine-mode natural aerosols ($\tau_n$) and marine aerosols ($\tau_m$) for four 5° longitudinal bands (see embedded maps), covering the Eastern Mediterranean based on MODIS Terra observations. Right column: latitudinal variability of dust extinction coefficients at 532 nm in $km^{-1}$ (color scale corresponds to the extinction coefficients and left $y$ axis to the atmospheric levels) and dust aerosol optical depth at 532 nm (dotted line corresponding to the right $y$ axis) for the same four bands from LIVAS CALIOP/CALIPSO observations.

**Table 4.** Relative contribution of anthropogenic aerosols, dust, fine-mode natural and marine aerosols to the total $AOD_{550}$ (bold) and the corresponding $\tau_a$, $\tau_d$, $\tau_n$ and $\tau_m$ levels with their $\pm 1\sigma$ values (in parentheses) over the Eastern Mediterranean (EMT), over the land-covered part (EML), over the oceanic part and over the nine subregions of the Eastern Mediterranean appearing in Fig. 1 based on the MODIS Terra and Aqua (italics) observations. The sum of the aerosol type AODs per region does not necessarily correspond to the total $AOD_{550}$ values appearing in Table 3 as these results were for the total of the days with aerosol retrievals, even for days when our aerosol type separation algorithm was not applicable.

| Region | Satellite | Contribution to MODIS TERRA/*AQUA* $AOD_{550}$ | | | |
|---|---|---|---|---|---|
| | | Anthropogenic | Dust | Fine-mode natural | Marine |
| EML | TERRA | **52** % (0.112 ± 0.087) | **32** % (0.074 ± 0.080) | **16** % (0.034 ± 0.026) | – |
| | *AQUA* | ***50*** *% (0.117 ± 0.093)* | ***35*** *% (0.090 ± 0.102)* | ***15*** *% (0.035 ± 0.028)* | – |
| EMO | TERRA | **41** % (0.086 ± 0.085) | **34** % (0.076 ± 0.185) | – | **25** % (0.054 ± 0.018) |
| | *AQUA* | ***40*** *% (0.079 ± 0.080)* | ***33*** *% (0.070 ± 0.181)* | – | ***27*** *% (0.054 ± 0.018)* |
| NBL | TERRA | **59** % (0.108 ± 0.101) | **23** % (0.042 ± 0.046) | **18** % (0.032 ± 0.030) | – |
| | *AQUA* | ***59*** *% (0.110 ± 0.100)* | ***24*** *% (0.045 ± 0.047)* | ***17*** *% (0.033 ± 0.030)* | – |
| SBL | TERRA | **55** % (0.109 ± 0.088) | **28** % (0.056 ± 0.058) | **17** % (0.033 ± 0.026) | – |
| | *AQUA* | ***55*** *% (0.113 ± 0.088)* | ***29*** *% (0.060 ± 0.060)* | ***16*** *% (0.034 ± 0.026)* | – |
| ANL | TERRA | **51** % (0.113 ± 0.075) | **34** % (0.076 ± 0.068) | **15** % (0.034 ± 0.023) | – |
| | *AQUA* | ***50*** *% (0.114 ± 0.075)* | ***35*** *% (0.079 ± 0.070)* | ***15*** *% (0.034 ± 0.023)* | – |
| NAL | TERRA | **50** % (0.113 ± 0.083) | **35** % (0.083 ± 0.085) | **15** % (0.034 ± 0.025) | – |
| | *AQUA* | ***48*** *% (0.118 ± 0.091)* | ***38*** *% (0.099 ± 0.108)* | ***14*** *% (0.035 ± 0.027)* | – |
| BSO | TERRA | **53** % (0.108 ± 0.103) | **22** % (0.044 ± 0.101) | – | **25** % (0.051 ± 0.016) |
| | *AQUA* | ***51*** *% (0.094 ± 0.087)* | ***22*** *% (0.042 ± 0.085)* | – | ***27*** *% (0.051 ± 0.016)* |
| NWO | TERRA | **41** % (0.087 ± 0.090) | **33** % (0.071 ± 0.142) | – | **26** % (0.055 ± 0.020) |
| | *AQUA* | ***40*** *% (0.079 ± 0.083)* | ***32*** *% (0.066 ± 0.127)* | – | ***28*** *% (0.055 ± 0.020)* |
| SWO | TERRA | **32** % (0.071 ± 0.070) | **42** % (0.097 ± 0.257) | – | **26** % (0.058 ± 0.018) |
| | *AQUA* | ***32*** *% (0.093 ± 0.288)* | ***41*** *% (0.072 ± 0.080)* | – | ***27*** *% (0.059 ± 0.018)* |
| NEO | TERRA | **48** % (0.098 ± 0.094) | **28** % (0.061 ± 0.144) | – | **24** % (0.050 ± 0.016) |
| | *AQUA* | ***46*** *% (0.086 ± 0.082)* | ***28*** *% (0.057 ± 0.115)* | – | ***26*** *% (0.050 ± 0.016)* |
| SEO | TERRA | **36** % (0.079 ± 0.070) | **39** % (0.087 ± 0.224) | – | **25** % (0.055 ± 0.016) |
| | *AQUA* | ***36*** *% (0.075 ± 0.071)* | ***38*** *% (0.080 ± 0.217)* | – | ***26*** *% (0.055 ± 0.016)* |

tal $AOD_{550}$ exhibits a low seasonal variability. The relative contribution of anthropogenic aerosols to the total $AOD_{550}$ ranges from 49 % in SON to 55 % in DJF based on Terra MODIS observations and from 48 % in MAM and SON to 52 % in JJA based on Aqua MODIS observations. In contrast, over the oceanic regions the relative contribution of $\tau_a$, $\tau_d$ and $\tau_m$ to the total $AOD_{550}$ exhibits a significant seasonal variability. The relative contribution of anthropogenic aerosols to the total $AOD_{550}$ ranges from 27 % / 27 % in DJF to 50 % / 47 % in JJA based on Terra/Aqua MODIS observations. The percentages appearing here are in accordance with the values appearing in Hatzianastassiou et al. (2009), where a different satellite-based approach was followed. Indicatively, for the greater Athens area, an average summertime anthropogenic contribution of ∼ 50 % was found here based on Terra MODIS data, which is within the summer period range of 47–61 % indicated in the study by Hatzianastassiou et al. (2009). In addition, the corresponding values for the greater Thessaloniki area, Crete, Cairo and Alexandria are 53, 38, 48 and 41 %, respectively, within the range of values (57–73, 36–52, 34–56 and 23–60 %) shown in Hatzianastassiou et al. (2009). Only in the case of Ankara do our results suggest a lower anthropogenic contribution (52 % vs. 71–84 %). Particularly for Athens, Gerasopoulos et al. (2011), following a different approach incorporating ground-based AOD observations and trajectory modeling, reached similar results (annual contribution of ∼ 62 % from local and regional sources and continental Europe, which is expected to be mostly of anthropogenic origin). Similarly, for Crete, Bergamo et al. (2008), using a different approach, also utilizing ground-based data, found an annual anthropogenic contribution of ∼ 43 %.

The seasonal patterns of the anthropogenic aerosols ($\tau_a$) over the Eastern Mediterranean based on MODIS Terra observations are presented in Fig. 11a, e, i and m, while the seasonal variability of $\tau_a$ over the whole region, over the land-covered part and the oceanic part and over the nine subregions of interest is presented in Fig. 12. The results based on MODIS Aqua observations are similar and can be found in Figs. S15a, e, i and m and S16. Generally, the local hot spots are detectable throughout the year; however, they are becoming much more discernible in spring and especially in summer. As shown in Fig. 12a, $\tau_a$ nearly doubles during the warm period of the year (spring–summer), with the seasonal variability being stronger over the sea (Fig. 12c) than over land (Fig. 12b). A clear peak is observed in summer, August being

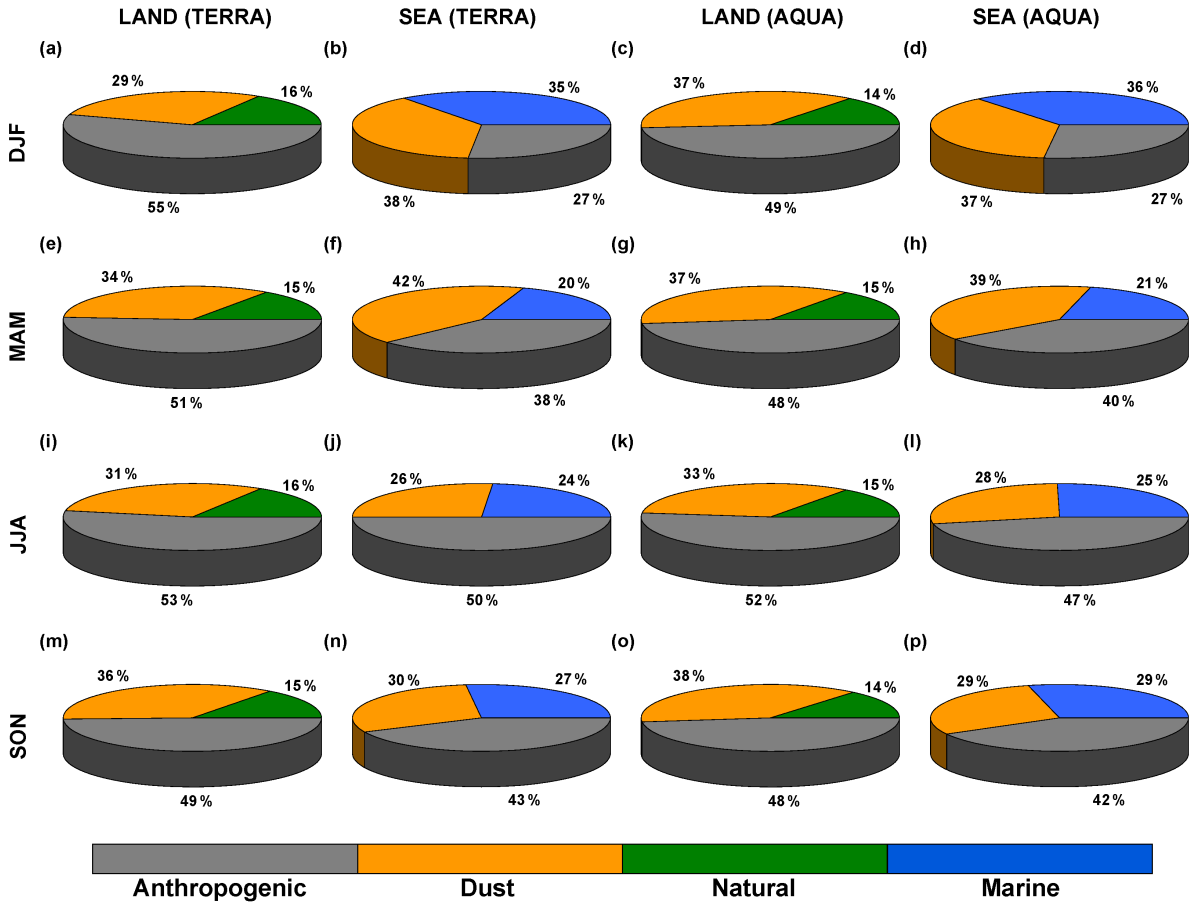


**Figure 10.** Seasonal relative contribution of anthropogenic aerosols, dust and fine-mode natural aerosols to the total $AOD_{550}$ over the land-covered part of the Eastern Mediterranean based on MODIS Terra **(a, e, i, m)** and MODIS Aqua **(c, g, k, o)** observations and seasonal relative contribution of anthropogenic aerosols, dust and marine aerosols to the total $AOD_{550}$ over the oceanic part of the Eastern Mediterranean based on MODIS Terra **(b, f, j, n)** and MODIS Aqua **(d, h, i, p)** observations.

the month with highest $\tau_a$ levels. As discussed in Sect. 4.3.1, the summer peak is mostly the result of three basic reasons. The first one is the deficiency of wet removal processes compared to the cold period. As shown in Fig. S17, based on the TRMM satellite observations, August and July are the months with the lowest precipitation levels over the land-covered part (a drop of $\sim 75$ % compared to winter months) and over the oceanic part (a drop of $\sim 90$ % compared to winter months) of the Eastern Mediterranean, respectively. The second reason is the enhancement of the photochemical production of secondary organic aerosols in summer (Kanakidou et al., 2011), and the third reason is the transport of pollution aerosols from central Europe and biomass burning aerosols from southwestern Russia and eastern Europe during the biomass burning season in July–August (Amiridis et al., 2010). The Etesians, which are persistent northerly winds that prevail over the Eastern Mediterranean during summer, bring dry and cool air masses and aerosols from the regions mentioned above while blocking, at the same time, the transport of desert dust in the region and dispersing local pollution in urban areas to levels typical for rural areas (see Tyrlis and Lelieveld, 2013, and references therein). As seen in Fig. 12a–l, a smaller but distinct, in most cases, $\tau_a$ peak appears in April, mostly as a result of the transport of biomass burning aerosols from Russia (across the latitudinal zone 45–55° N). This is in line with the findings of Sciare et al. (2008) who detected traces of these biomass burning aerosols over the island of Crete in southern Greece.

As discussed above, the relative contribution of dust to the total $AOD_{550}$ over land exhibits a low seasonal variability ranging from 29 % in DJF to 36 % in SON based on Terra MODIS observations and from 33 % in JJA to 38 % in SON based on Aqua MODIS observations (see Fig. 10). Over the oceanic regions the relative contribution of dust to the total $AOD_{550}$ ranges significantly throughout a year from 26 % / 28 % in JJA to 42 % / 39 % in MAM based on Terra/Aqua MODIS observations. The percentages appearing here are in accordance with model and obser-

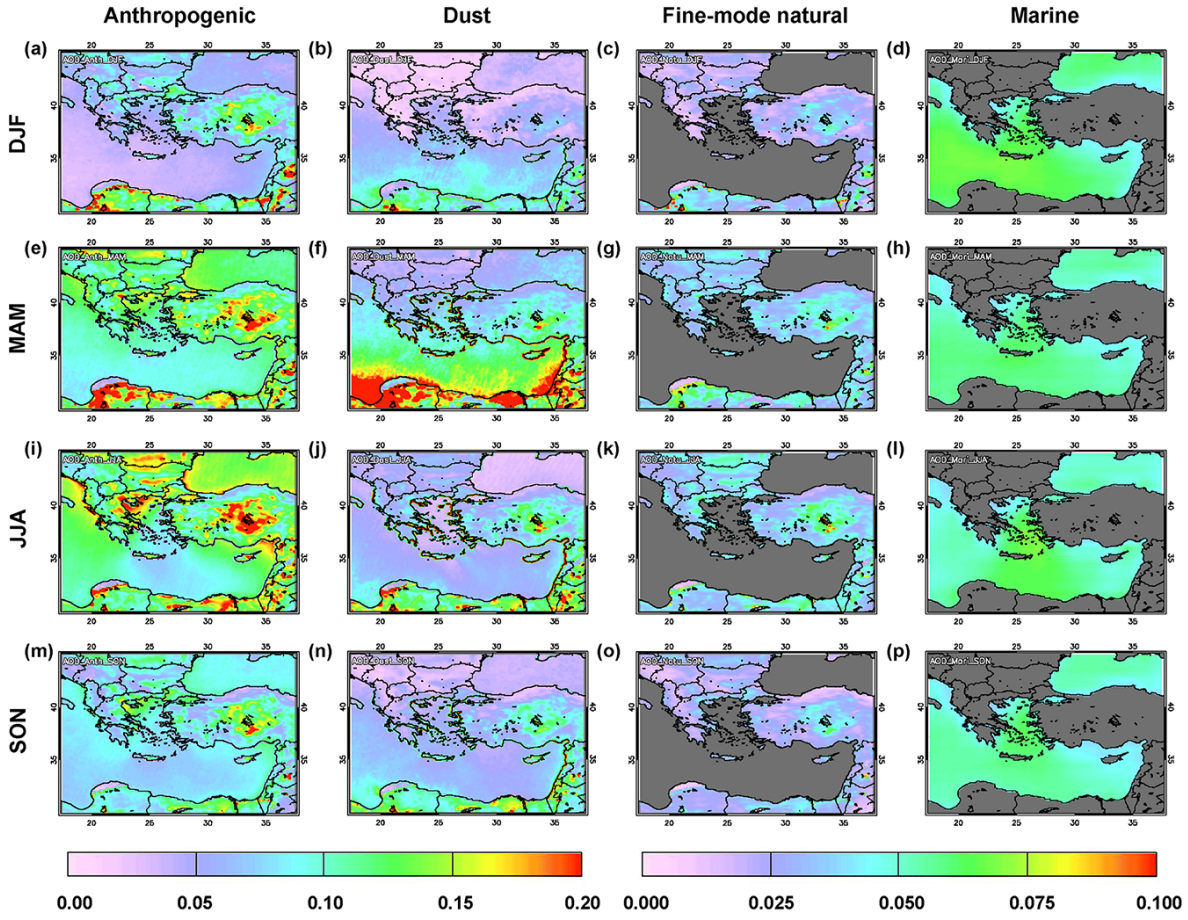


**Figure 11.** Seasonal **(a, e, i, m)** anthropogenic aerosol ($\tau_a$), **(b, f, j, n)** dust ($\tau_d$), **(c, g, k, o)** fine-mode natural aerosol ($\tau_n$) and **(d, h, i, p)** marine aerosol ($\tau_m$) patterns over the Eastern Mediterranean based on MODIS Terra observations during the period March 2000–December 2012 (March 2000–December 2007 for regions of northern Africa covered by DB data only).

vational studies. For example, de Meij et al. (2012), using the atmospheric chemistry general circulation model EMAC (ECHAM/MESSy Atmospheric Chemistry), showed that dust contributes on an annual level $\sim 30\,\%$ to the total $AOD_{550}$ over stations located in the area of the Eastern Mediterranean. Gerasopoulos et al. (2011) found a $\sim 23\,\%$ contribution of northern African dust to the total AOD over Athens using ground-based AOD observations and trajectory modeling. Taking into account that part of the $\sim 39\,\%$ local and regional sources appearing in Gerasopoulos et al. (2011) is due to local dust sources, especially in summer, it turns out that their results are in agreement with the $\sim 33\,\%$ relative contribution found in this work for the greater Athens area based on Terra MODIS observations. The seasonal patterns of dust ($\tau_d$) over the region based on Terra MODIS observations are shown in Fig. 11b, f, j and n, while the seasonal variability of $\tau_d$ over the whole region, over land, over the sea and over the nine subregions of interest is shown in Fig. 12. The corresponding results based on MODIS Aqua observations are pretty similar and can be found in Figs. S15b, f, j and n and S16.

As seen in Fig. 11f, in spring, mostly due to the strong Sahara dust events, very high $\tau_d$ values appear over land regions in northern Africa, Middle East, Anatolia and oceanic areas across the Eastern Mediterranean (especially below 35° N). Dust loading over the sea exhibits two maxima, one at the coastal zone of Libya and one across the coastal zone of Middle East. The same two maxima, but with much lower $\tau_d$ values, appear in summer (Fig. 11j) and autumn (Fig. 11n). Over land, the $\tau_d$ patterns are similar in summer and autumn, the maximum values appearing over the Anatolian Plateau and areas of northern Africa and Middle East. During winter, dust maxima appear across the coastal zone of northern Africa, with relatively low $\tau_d$ values across the coastal zone of Middle East (Fig. 11b). In winter $\tau_d$ levels are as low over land compared to the other seasons (Fig. 11b, f, j and n) as precipitation levels (see Fig. S17), and hence the wet scavenging of aerosols peaks. At the same time, the local emissions of dust are low for regions away from the large area sources in

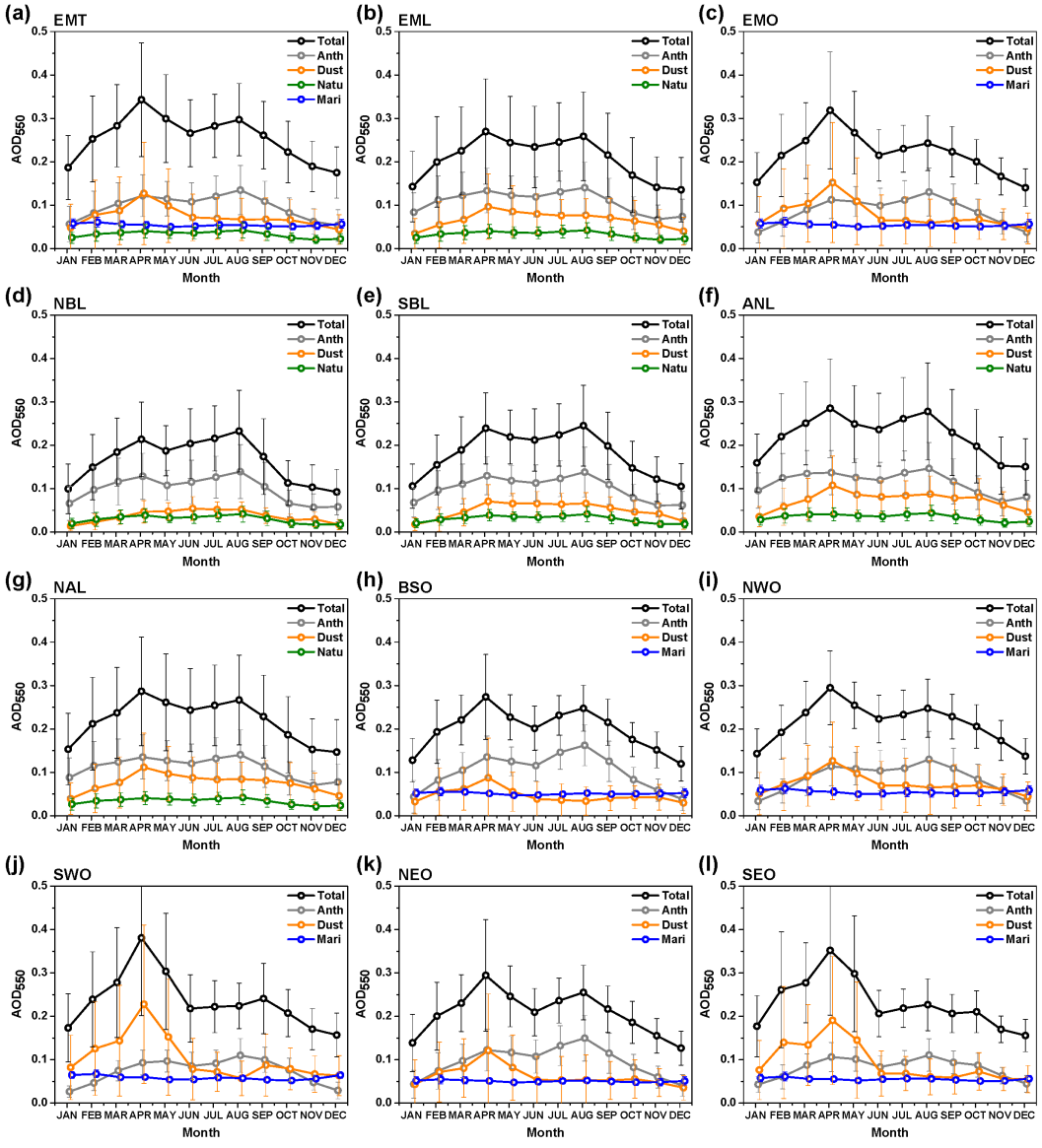


**Figure 12.** Seasonal variability of anthropogenic aerosols ($\tau_a$), dust ($\tau_d$), fine-mode natural aerosols ($\tau_n$) and marine aerosols ($\tau_m$) over the Eastern Mediterranean (EMT), over the land-covered part (EML), over the oceanic part (EMO) and over the nine subregions of the Eastern Mediterranean appearing in Fig. 1 based on MODIS Terra observations. The error bars represent the $\pm 1\sigma$ values calculated from monthly gridded data.

the south (Liora et al., 2015). In contrast, over the sea, $\tau_d$ levels in winter are similar to or slightly higher for some areas than those in summer and autumn (see Figs. 11 and 12) as this is the season with the second highest frequency (after spring) of strong ($\sim 21\,\%$) and extreme ($\sim 26\,\%$) desert dust episodes in the region (see Gkikas et al., 2013, for details). February is by far the winter month with the highest $\tau_d$ levels (see Fig. 12) in line with the findings of Pey et al. (2013), who showed that the intensity of African dust episodes over stations in Greece and Cyprus peaks in February. Dust exhibits a strong peak in spring, April being the month with the highest $\tau_d$ levels in line with other studies (e.g., Israelevic et al., 2012; Varga et al., 2014). The peak in April is a result of the high cyclonic activity over northern Africa during this month as shown by Flaounas et al. (2015). According to the same study, low-pressure systems are responsible for $\sim 10$–$20\,\%$ of moderate and $\sim 40$–$50\,\%$ of high and extreme Sahara dust transport events over the Eastern Mediterranean. Northern Africa (Sharav) cyclones develop mainly in spring and summer, while Mediterranean cyclones develop in winter and autumn. The Mediterranean cyclones are more intense than Sharav cyclones. The region is also af-

fected by events bringing particles from dust source regions in the eastern part of the Mediterranean Basin (Negev desert in Israel, Sinai in Egypt, Anatolian Plateau in Turkey) and the Arabian deserts (Basart et al., 2009; Pey et al., 2013; Abdelkader et al., 2015). Dust remains in the atmosphere for a period of 1–4 days undergoing chemical aging before being removed (see Abdelkader et al., 2015, and references therein). The seasonal variability of $\tau_d$ is much stronger and the spring maxima much more prominent over the sea (see Fig. 12). This is expected, as dust is only occasionally transported over the sea during episodic events, while over land, local sources also contribute to the dust burden, especially in summer due to the dryness of soil. For example, over NBL, a broad spring-summer peak is observed, June being the month with the highest $\tau_d$ levels. As one moves south (SBL, ANL and NAL) the April peak becomes more prominent.

The relative contribution of fine-mode natural aerosols to the total $AOD_{550}$ over land exhibits a very low seasonal variability, ranging from 15 % in MAM and SON to 16 % in DJF and JJA based on Terra MODIS observations and from 14 % in DJF and SON to 15 % in MAM and JJA based on Aqua MODIS observations (see Fig. 10). The seasonal variability is also very low, the highest values appearing in spring and summer (Fig. 12). Despite the generally low contribution of fine-mode natural aerosols to the total $AOD_{550}$ over the Eastern Mediterranean, $\tau_n$ levels are similar to $\tau_d$ levels during winter months over specific regions (NBL and SBL). The low seasonal variability can also be seen in Fig. 11c, g, k and o where the patterns of fine-mode natural aerosols ($\tau_n$) are presented.

The seasonal relative contribution of marine aerosols to the total $AOD_{550}$ over the oceanic regions of the Eastern Mediterranean is shown in Fig. 10. $\tau_m$ ranges from 20 % in MAM to 35 % in DJF based on Terra MODIS observations and from 21 % in MAM to 36 % in DJF based on Aqua MODIS observations (see Fig. 10). Like in the case of fine-mode natural aerosols, the seasonal variability is very low, but here the highest values appear in winter (Fig. 12). Due to the linear relation of $\tau_m$ and near-surface wind speed within our algorithm (see Fig. 2), the $\tau_m$ seasonal variability and patterns follow the wind speed ones (see Figs. 11d, h, l and p and S14). Marine aerosol concentrations are lower close to the coastlines, while the highest concentrations (see Liora et al., 2015) and $\tau_m$ values within the Eastern Mediterranean appear over the Aegean Sea (see Fig. 11). Overall, the $\tau_m$ patterns are in accordance with the $\tau_m$, marine particulate matter concentration and sea salt emission patterns from previous studies (Im et al., 2012; Nabat et al., 2013; Rea et al., 2015; Liora et al., 2015).

## 5 Summary and conclusions

In this work, satellite data from MODIS Terra (March 2000–December 2012) and Aqua (July 2002–December 2012) were analyzed separately in order to examine the spatial and temporal variability of aerosols over the Eastern Mediterranean. A high-resolution ($0.1° \times 0.1°$) MODIS gridded dataset was compiled using a method that could be used in future regional studies. A number of tests were implemented, and the dataset was validated in detail using sun photometric observations from 13 AERONET stations. According to the validation, the statistics appearing for MODIS Terra throughout the paper could be considered more robust, while areas in northern Africa are expected to be affected by the extended use of DB data, which do not exhibit a very good matching with the ground-based observations. It is shown that the gridding method we use offers the best compromise for studying the spatial variability of aerosols on a regional or local scale, preserving, at the same time, the representativeness of the real aerosol load over each specific spot.

Based on MODIS observations, the average $AOD_{550}$ levels over the region of the Eastern Mediterranean are $\sim 0.22 \pm 0.19$, which is $\sim 45$ % higher than the global mean. A number of aerosol hot spots that coincide with megacities, large- and even medium-sized cities, industrial zones, power plant complexes, river basins, etc., can be detected on the AOD maps. A number of local aerosol sources can also be seen on satellite retrieved tropospheric $NO_2$ and planetary boundary layer $SO_2$ maps from OMI/AURA. This is indicative of the strong presence of anthropogenic aerosols over these regions. Topography and precipitation also play an important role. Generally, regions with mountain ranges are characterized by low AODs, while regions of low altitude are characterized by higher AODs. Regions with high $AOD_{550}$ are, in many cases, connected to low precipitation levels and vice versa. Precipitation is the major washout mechanism of atmospheric pollutants. Low removal rates from precipitation contribute in preserving the high $AOD_{550}$ levels that are a result of emissions and other atmospheric processes.

The $AOD_{550}$ patterns over the Eastern Mediterranean exhibit a significant seasonal variability, which is mostly driven by precipitation, photochemical production of secondary organic aerosols, transport of pollution and biomass burning aerosols from central and eastern Europe and transport of dust from the Sahara and the Middle East. Differences between the MODIS Terra and Aqua Collection 051 $AOD_{550}$ over the Eastern Mediterranean are generally small ($\sim -8$ % over land and $\sim 5$ % over the sea). The comparison of the Terra–Aqua differences with diurnal variabilities from the AERONET stations showed that only a part of the observed differences is due to the diurnal variability of aerosols.

The MODIS data were combined with data from other satellites (Earth Probe TOMS, OMI/AURA), reanalysis projects (ERA-Interim, MACC) and a chemistry–aerosol-transport model (GOCART) to calculate the contribution of different types of aerosols to the total $AOD_{550}$. The algorithm used was optimized for the Eastern Mediterranean through a number of tests and comparison with LIVAS

CALIOP/CALIPSO dust retrievals and AERONET ground-based observations. A different approach is used for land and sea as there is not any reliable satellite-retrieved quantity to separate the contribution of fine- and coarse-mode aerosols over land surfaces.

Overall, for the land areas, based on MODIS Terra observations, 52 % ($0.112 \pm 0.087$) of the total $AOD_{550}$ is due to anthropogenic aerosols, 32 % ($0.074 \pm 0.080$) due to dust and 16 % ($0.034 \pm 0.026$) due to fine-mode natural aerosols (see Fig. 7). For the oceanic areas, 41 % ($0.086 \pm 0.085$) of the total $AOD_{550}$ is due to anthropogenic aerosols, 34 % ($0.076 \pm 0.185$) due to dust and 25 % ($0.054 \pm 0.018$) due to marine aerosols. The results based on observations from MODIS Aqua are similar to the MODIS Terra ones and are in accordance with previous studies.

Over land, the $\tau_a$ maxima are detected over local particle pollution sources (cities, industrial zones, etc.). Over the sea, $\tau_a$ is higher along the coasts, being significantly lower at greater distance. Very high $\tau_d$ values appear over land regions in northern Africa, the Middle East, Anatolia and oceanic areas across the Eastern Mediterranean, especially for latitudes below 35° N. Over the sea, dust loading exhibits two maxima, one at the coastal zone of Libya and one across the coastal zone of the Middle East. $\tau_d$ decreases with distance from the large dust sources in the south and southeast. Generally, dust reaches heights of up to $\sim$4–5 km in the area, the largest fraction of dust mass being confined within the first 2–3 km of the troposphere. The spatial variability of $\tau_n$ and $\tau_m$ is very low compared to $\tau_a$ and $\tau_d$, following the total $AOD_{550}$ patterns and the near-surface wind speed patterns, respectively.

Over land, the relative contribution of anthropogenic aerosols, dust and fine-mode natural aerosols to the total $AOD_{550}$ exhibits a low seasonal variability, while over the sea the relative contribution of anthropogenic aerosols, dust and marine aerosols shows a significant seasonal variability.

$\tau_a$ nearly doubles during the warm period of the year (spring–summer), August and April being the months with the highest $\tau_a$ levels. The summer peak is mostly the result of low precipitation levels, enhancement of the photochemical production of secondary organic aerosols and the transport of pollution aerosols from central Europe and biomass burning aerosols from southwestern Russia and eastern Europe during the biomass burning season in July–August. The spring maximum in April is mostly the result of transport of biomass burning aerosols from Russia in line with previous studies. Dust exhibits a strong peak in spring (April), especially over the southern regions. April is the month with the highest $\tau_d$ levels as a result of the high cyclonic activity over northern Africa. The seasonal variability of dust is much stronger, and the spring maxima are much more prominent over the sea as dust is only occasionally transported there during episodic events, while over land, local sources contribute to the dust burden, especially in summer due to the soil dryness. The seasonal variability of fine-mode natural aerosols is very low, the highest values appearing in spring and summer. Marine aerosols also present a very low seasonal variability, the highest values appearing in winter due to the high near-surface wind speeds.

Overall, it is suggested that the $AOD_{550}$, $\tau_a$, $\tau_d$, $\tau_n$ and $\tau_m$ high-resolution gridded dataset that was compiled in this work could be used in a number of future atmospheric and biological studies focusing on the region of the Eastern Mediterranean (e.g., satellite- and ground-based studies on aerosol–cloud–radiation interactions, experimental and field campaign studies on aerosols and clouds and research on the impact of aerosols on human health and nature). It is also acknowledged that a future update of the results presented here using more recent releases of MODIS aerosol data (e.g., Collection 6) and aerosol reanalysis datasets (e.g., NASA's Modern-Era Retrospective analysis for Research and Applications Aerosol Reanalysis) would be a useful contribution.

## 6 Data availability

The level-2 MODIS Terra (MOD04_L2) and MODIS Aqua (MYD04_L2) Collection 051 data have been acquired through NASA's Level 1 and Atmosphere Archive and Distribution System (LAADS) (http://ladsweb.nascom.nasa.gov). The version 2.0 level 2.0 high-quality cloud screened data from 13 AERONET ground stations in the region of the Eastern Mediterranean have been acquired through http://aeronet.gsfc.nasa.gov. The LIVAS CALIOP/CALIPSO data were produced and provided by the co-authors of this paper, who are affiliated with the National Observatory of Athens. Part of the data are available on the LIVAS website: http://lidar.space.noa.gr:8080/livas/. All the Earth Probe TOMS and OMI/AURA observations (AI, $NO_2$ and $SO_2$) used here were acquired through NASA's GIOVANNI web database (http://giovanni.gsfc.nasa.gov/giovanni/). The ERA-Interim reanalysis data were acquired through ECMWF's website (http://apps.ecmwf.int/datasets/data/interim-full-daily/). The MACC reanalysis data were downloaded from http://apps.ecmwf.int/datasets/data/macc-reanalysis/. The GOCART data were acquired from an older version of NASA's GIOVANNI web database (http://disc.sci.gsfc.nasa.gov/giovanni/). The 3B43 TRMM and Other Sources Monthly Rainfall Product (version 7) data were taken from GIOVANNI (http://giovanni.gsfc.nasa.gov/giovanni/). The dataset produced in this work by combining data from the sources mentioned above may be available by contacting the corresponding author of this paper.

**The Supplement related to this article is available online at doi:10.5194/acp-16-13853-2016-supplement.**

*Acknowledgements.* This research received funding from the European Social Fund (ESF) and national resources under the operational programme Education and Lifelong Learning (EdLL) within the framework of the Action "Supporting Postdoctoral Researchers" (QUADIEEMS project), from the European Research Council under the European Union's Seventh Framework Programme (FP7/2007-2013)/ERC grant agreement no. 226144 (C8 project), from the FP7 Programme MarcoPolo (grant number 606953, theme SPA.2013.3.2-01) and from the European Union's Horizon 2020 Research and Innovation programme under grant agreement no. 654109. The authors express their gratitude to the teams that developed the algorithms and produced the satellite products used in this study, and to those who worked on the production of the model and reanalysis data used here. Special thanks are expressed to NASA Goddard Space Flight Center (GSFC) Level 1 and Atmosphere Archive and Distribution System (LAADS) (http://ladsweb.nascom.nasa.gov) for making the MODIS Terra and Aqua Collection 051 level-2 aerosol data available, and the principal investigators and staff for maintaining the 13 AERONET (http://aeronet.gsfc.nasa.gov) sites used in the present work. LIVAS has been financed under the ESA-ESTEC project LIVAS (contract no. 4000104106/11/NL/FF/fk). We thank the ICARE Data and Services Center (www.icare.univ-lille1.fr) for providing access to NASA's CALIPSO data, and acknowledge the use of NASA's CALIPSO data. Special thanks are expressed to ECMWF (www.ecmwf.int) for the provision of the ERA-Interim and MACC reanalysis data. NASA's GIOVANNI web database (http://giovanni.gsfc.nasa.gov/giovanni/) is highly acknowledged for the provision of Aerosol Index data from Earth Probe TOMS and OMI, aerosol data from the GOCART chemistry–aerosol-transport model (older version of GIOVANNI), tropospheric $NO_2$ and PBL $SO_2$ columnar data from OMI and precipitation data from 3B43 TRMM and Other Sources Monthly Rainfall Product. Aristeidis K. Georgoulias acknowledges the fruitful discussions with various colleagues from the Max Planck Institute for Chemistry and the Cyprus Institute (EEWRC), who indirectly contributed to this research.

The article processing charges for this open-access publication were covered by the Max Planck Society.

Edited by: S. Kazadzis
Reviewed by: three anonymous referees

## References

Abdelkader, M., Metzger, S., Mamouri, R. E., Astitha, M., Barrie, L., Levin, Z., and Lelieveld, J.: Dust-air pollution dynamics over the eastern Mediterranean, Atmos. Chem. Phys., 15, 9173–9189, doi:10.5194/acp-15-9173-2015, 2015.

Acker, J. G. and Leptoukh, G.: Online analysis enhances use of NASA Earth science data, Eos T. AGU, 88, 14–17, doi:10.1029/2007EO020003, 2007.

Alexandersson, H.: A homogeneity test applied to precipitation data, J. Climatol., 6, 661–675, doi:10.1002/joc.3370060607, 1986.

Alexandri, G., Georgoulias, A. K., Zanis, P., Katragkou, E., Tsikerdekis, A., Kourtidis, K., and Meleti, C.: On the ability of RegCM4 regional climate model to simulate surface solar radiation patterns over Europe: an assessment using satellite-based observations, Atmos. Chem. Phys., 15, 13195–13216, doi:10.5194/acp-15-13195-2015, 2015.

Alpert, P. and Ganor, E.: Sahara mineral dust measurements from TOMS: Comparison to surface observations over the Middle East for the extreme dust storm, 14–17 March 1998, J. Geophys. Res., 106, 18275–18286, doi:10.1029/2000JD900366, 2001.

Amiridis V., Balis, D., Kazadzis, S., Giannakaki, E., Papayannis, A., and Zerefos, C.: Four years aerosol observations with a Raman lidar at Thessaloniki, Greece, in the framework of European Aerosol Research Lidar Network (EARLINET), J. Geophys. Res., 110, D21203, doi:10.1029/2005JD006190, 2005.

Amiridis, V., Balis, D. S., Giannakaki, E., Stohl, A., Kazadzis, S., Koukouli, M. E., and Zanis, P.: Optical characteristics of biomass burning aerosols over Southeastern Europe determined from UV-Raman lidar measurements, Atmos. Chem. Phys., 9, 2431–2440, doi:10.5194/acp-9-2431-2009, 2009.

Amiridis, V., Giannakaki, E., Balis, D. S., Gerasopoulos, E., Pytharoulis, I., Zanis, P., Kazadzis, S., Melas, D., and Zerefos, C.: Smoke injection heights from agricultural burning in Eastern Europe as seen by CALIPSO, Atmos. Chem. Phys., 10, 11567–11576, doi:10.5194/acp-10-11567-2010, 2010.

Amiridis, V., Wandinger, U., Marinou, E., Giannakaki, E., Tsekeri, A., Basart, S., Kazadzis, S., Gkikas, A., Taylor, M., Baldasano, J., and Ansmann, A.: Optimizing CALIPSO Saharan dust retrievals, Atmos. Chem. Phys., 13, 12089–12106, doi:10.5194/acp-13-12089-2013, 2013.

Amiridis, V., Marinou, E., Tsekeri, A., Wandinger, U., Schwarz, A., Giannakaki, E., Mamouri, R., Kokkalis, P., Binietoglou, I., Solomos, S., Herekakis, T., Kazadzis, S., Gerasopoulos, E., Proestakis, E., Kottas, M., Balis, D., Papayannis, A., Kontoes, C., Kourtidis, K., Papagiannopoulos, N., Mona, L., Pappalardo, G., Le Rille, O., and Ansmann, A.: LIVAS: a 3-D multi-wavelength aerosol/cloud database based on CALIPSO and EARLINET, Atmos. Chem. Phys., 15, 7127–7153, doi:10.5194/acp-15-7127-2015, 2015.

Antoine, D. and Nobileau, D.: Recent increase of Saharan dust transport over the Mediterranean Sea, as revealed from ocean color satellite (SeaWiFS) observations, J. Geophys. Res., 111, D12214, doi:10.1029/2005JD006795, 2006.

Athanassiou, G., Hatzianastassiou, N., Gkikas, A., and Papadimas, C. D.: Estimating aerosol optical depth over the broader greek area from MODIS satellite, Water Air Soil. Poll., 224, 1605, doi:10.1007/s11270-013-1605-2, 2013.

Balis, D., Amiridis, V., Nickovic, S., Papayannis, A., and Zerefos, C.: Optical properties of Saharan dust layers as detected by a Raman lidar at Thessaloniki, Greece, Geophys. Res. Lett., 31, D23S90, doi:10.1029/2004GL019881, 2004.

Barnaba, F. and Gobbi, G. P.: Aerosol seasonal variability over the Mediterranean region and relative impact of maritime, continental and Saharan dust particles over the basin from MODIS data in the year 2001, Atmos. Chem. Phys., 4, 2367–2391, doi:10.5194/acp-4-2367-2004, 2004.

Basart, S., Pérez, C., Cuevas, E., Baldasano, J. M., and Gobbi, G. P.: Aerosol characterization in Northern Africa, Northeastern Atlantic, Mediterranean Basin and Middle East from direct-sun AERONET observations, Atmos. Chem. Phys., 9, 8265–8282, doi:10.5194/acp-9-8265-2009, 2009.

Bellouin, N., Jones, A., Haywood, J., and Christopher, S. A.: Updated estimate of aerosol direct radiative forcing from satellite observations and comparison against the Hadley Centre climate model, J. Geophys. Res., 113, D10205, doi:10.1029/2007JD009385, 2008.

Bellouin, N., Quaas, J., Morcrette, J.-J., and Boucher, O.: Estimates of aerosol radiative forcing from the MACC re-analysis, Atmos. Chem. Phys., 13, 2045–2062, doi:10.5194/acp-13-2045-2013, 2013.

Benas, N., Hatzianastassiou, N., Matsoukas, C., Fotiadi, A., Mihalopoulos, N., and Vardavas, I.: Aerosol shortwave direct radiative effect and forcing based on MODIS Level 2 data in the Eastern Mediterranean (Crete), Atmos. Chem. Phys., 11, 12647–12662, doi:10.5194/acp-11-12647-2011, 2011.

Benas, N., Beloconi, A., and Chrysoulakis, N.: Estimation of urban PM10 concentration, based on MODIS and MERIS/AATSR synergistic observations, Atmos. Environ., 79, 448–454, doi:10.1016/j.atmosenv.2013.07.012, 2013.

Benedetti, A., Morcrette, J.-J., Boucher, O., Dethof, A., Engelen, R. J., Fisher, M., Flentjes, H., Huneeus, N., Jones, L., Kaiser, J. W., Kinne, S., Mangold, A., Razinger, M., Simmons, A. J., Suttie, M., and the GEMS-AER team: Aerosol analysis and forecast in the ECMWF Integrated Forecast System. Part II: Data assimilation, J. Geophys. Res., 114, D13205, doi:10.1029/2008JD011115, 2009.

Bergamo, A., Tafuro, A. M., Kinne, S., De Tomasi, F., and Perrone, M. R.: Monthly-averaged anthropogenic aerosol direct radiative forcing over the Mediterranean based on AERONET aerosol properties, Atmos. Chem. Phys., 8, 6995–7014, doi:10.5194/acp-8-6995-2008, 2008.

Bucsela, E. J., Krotkov, N. A., Celarier, E. A., Lamsal, L. N., Swartz, W. H., Bhartia, P. K., Boersma, K. F., Veefkind, J. P., Gleason, J. F., and Pickering, K. E.: A new stratospheric and tropospheric $NO_2$ retrieval algorithm for nadir-viewing satellite instruments: applications to OMI, Atmos. Meas. Tech., 6, 2607–2626, doi:10.5194/amt-6-2607-2013, 2013.

Burton, S. P., Ferrare, R. A., Vaughan, M. A., Omar, A. H., Rogers, R. R., Hostetler, C. A., and Hair, J. W.: Aerosol classification from airborne HSRL and comparisons with the CALIPSO vertical feature mask, Atmos. Meas. Tech., 6, 1397–1412, doi:10.5194/amt-6-1397-2013, 2013.

Carmona, I. and Alpert, P.: Synoptic classification of Moderate Resolution Imaging Spectroradiometer aerosols over Israel, J. Geophys. Res., 114, D07208, doi:10.1029/2008JD010160, 2009.

Cesnulyte, V., Lindfors, A. V., Pitkänen, M. R. A., Lehtinen, K. E. J., Morcrette, J.-J., and Arola, A.: Comparing ECMWF AOD with AERONET observations at visible and UV wavelengths, Atmos. Chem. Phys., 14, 593–608, doi:10.5194/acp-14-593-2014, 2014.

Chin, M., Rood, R. B., Lin, S.-J., Müller, J.-F., and Thompson, A. M.: Atmospheric sulfur cycle simulated in the global model GOCART: Model description and global properties, J. Geophys. Res., 105, 24671, doi:10.1029/2000JD900384, 2000.

Chin, M., Ginoux, P., Kinne, S., Torres, O., Holben, B. N., Duncan, B. N., Martin, R. V., Logan, J. A., Higurashi, A., and Nakajima, T.: Tropospheric Aerosol Optical Thickness from the GOCART Model and Comparisons with Satellite and Sun Photometer Measurements, J. Atmos. Sci., 59, 461–483, doi:10.1175/1520-0469(2002)059<0461:TAOTFT>2.0.CO;2, 2002.

Chin, M., Chu, A., Levy, R., Remer, L., Kaufman, Y., Holben, B., Eck, T., Ginoux, P., and Gao, Q.: Aerosol distribution in the Northern Hemisphere during ACE-Asia: Results from global model, satellite observations, and Sun photometer measurements, J. Geophys. Res.-Atmos., 109, L13104, doi:10.1029/2004JD004829, 2004.

Chin, M., Diehl, T., Ginoux, P., and Malm, W.: Intercontinental transport of pollution and dust aerosols: implications for regional air quality, Atmos. Chem. Phys., 7, 5501–5517, doi:10.5194/acp-7-5501-2007, 2007.

Chin, M., Diehl, T., Dubovik, O., Eck, T. F., Holben, B. N., Sinyuk, A., and Streets, D. G.: Light absorption by pollution, dust, and biomass burning aerosols: a global model study and evaluation with AERONET measurements, Ann. Geophys., 27, 3439–3464, doi:10.5194/angeo-27-3439-2009, 2009.

Chu, D. A., Kaufman, Y. J., Ichoku, C., Remer, L. A., Tanre, D., and Holben, B. N.: Validation of MODIS aerosol optical depth retrieval over land, Geophys. Res. Lett., 29, 8007, doi:10.1029/2001GL013205, 2002.

Cuevas, E., Camino, C., Benedetti, A., Basart, S., Terradellas, E., Baldasano, J. M., Morcrette, J. J., Marticorena, B., Goloub, P., Mortier, A., Berjón, A., Hernández, Y., Gil-Ojeda, M., and Schulz, M.: The MACC-II 2007–2008 reanalysis: atmospheric dust evaluation and characterization over northern Africa and the Middle East, Atmos. Chem. Phys., 15, 3991–4024, doi:10.5194/acp-15-3991-2015, 2015.

de Meij, A. and Lelieveld, J.: Evaluating aerosol optical properties observed by ground-based and satellite remote sensing over the Mediterranean and the Middle East in 2006, Atmos. Res., 99, 415–433, doi:10.1016/j.atmosres.2010.11.005, 2011.

de Meij, A., Pozzer, A., Pringle, K. J., Tost, H., and Lelieveld, J.: EMAC model evaluation and analysis of atmospheric aerosol properties and distribution, Atmos. Res, 114–115, 38–69, 2012.

Dee, D. P., Uppala, S. M., Simmons, A. J., Berrisford, P., Poli, P., Kobayashi, S., Andrae, U., Balmaseda, M. A., Balsamo, G., Bauer, P., Bechtold, P., Beljaars, A. C. M., van de Berg, L., Bidlot, J., Bormann, N., Delsol, C., Dragani, R., Fuentes, M., Geer, A. J., Haimberger, L., Healy, S. B., Hersbach, H., Hólm, E. V., Isaksen, L., Kållberg, P., Köhler, M., Matricardi, M., Mcnally, A. P., Monge-Sanz, B. M., Morcrette, J. J., Park, B. K., Peubey, C., de Rosnay, P., Tavolato, C., Thépaut, J. N., and Vitart, F.: The ERA-Interim reanalysis: Configuration and performance of the data assimilation system, Q. J. Roy. Meteor. Soc., 137, 553–597, doi:10.1002/qj.828, 2011.

Derimian, Y., Karnieli, A., Kaufman, Y. J., Andreae, M. O., Andreae, T. W., Dubovik, O., Maenhaut, W., Koren, I., and Holben, B. N.: Dust and pollution aerosols over the Negev desert, Israel: Properties, transport, and radiative effect, J. Geophys. Res., 111, D05205, doi:10.1029/2005JD006549, 2006.

Dubovik, O. and King, M. D.: A flexible inversion algorithm for retrieval of aerosol optical properties from Sun and sky radiance measurements, J. Geophys. Res., 105, 20673, doi:10.1029/2000JD900282, 2000.

Dubovik, O., Smirnov, A., Holben, B. N., King, M. D., Kaufman, Y. J., Eck, T. F., and Slutsker, I.: Accuracy assessments of aerosol optical properties retrieved from Aerosol Robotic Network (AERONET) Sun and sky radiance measurements, J. Geophys. Res., 105, 9791, doi:10.1029/2000JD900040, 2000.

Dubovik, O., Holben, B., Eck, T. F., Smirnov, A., Kaufman, Y. J., King, M. D., Tanré, D., and Slutsker, I.: Variability of Absorption and Optical Properties of Key Aerosol Types Observed in Worldwide Locations, J. Atmos. Sci., 59, 590–608, doi:10.1175/1520-0469(2002)059<0590:VOAAOP>2.0.CO;2, 2002.

Eck, T. F., Holben, B. N., Reid, J. S., Dubovik, O., Smirnov, A., O'Neill, N. T., Slutsker, I., and Kinne, S.: Wavelength dependence of the optical depth of biomass burning, urban, and desert dust aerosols, J. Geophys. Res., 104, 31333–31349, doi:10.1029/1999jd900923, 1999.

Elguindi, N., Clark, H., Ordóñez, C., Thouret, V., Flemming, J., Stein, O., Huijnen, V., Moinat, P., Inness, A., Peuch, V.-H., Stohl, A., Turquety, S., Athier, G., Cammas, J.-P., and Schultz, M.: Current status of the ability of the GEMS/MACC models to reproduce the tropospheric CO vertical distribution as measured by MOZAIC, Geosci. Model Dev., 3, 501–518, doi:10.5194/gmd-3-501-2010, 2010.

El-Metwally, M. and Alfaro, S. C.: Correlation between meteorological conditions and aerosol characteristics at an East-Mediterranean coastal site, Atmos. Res., 132–133, 76–90, doi:10.1016/j.atmosres.2013.05.006, 2013.

El-Metwally, M., Alfaro, S. C., Abdel Wahab, M. M., Zakey, A. S., and Chatenet, B.: Seasonal and inter-annual variability of the aerosol content in Cairo (Egypt) as deduced from the comparison of MODIS aerosol retrievals with direct AERONET measurements, Atmos. Res., 97, 14–25, doi:10.1016/j.atmosres.2010.03.003, 2010.

Flaounas, E., Kotroni, V., Lagouvardos, K., Kazadzis, S., Gkikas, A., and Hatzianastassiou, N.: Cyclone contribution to dust transport over the Mediterranean region, Atmos. Sci. Lett., 16, 473–478, doi:10.1002/asl.584, 2015.

Georgoulias, A. K. and Kourtidis, K. A.: On the aerosol weekly cycle spatiotemporal variability over Europe, Atmos. Chem. Phys., 11, 4611–4632, doi:10.5194/acp-11-4611-2011, 2011.

Georgoulias, A. K. and Kourtidis, K. A.: A high resolution satellite view of the aerosol weekly cycle variability over Central Europe, Atmos. Res., 107, 145–160, doi:10.1016/j.atmosres.2012.01.003, 2012.

Georgoulias, A. K., Balis, D., Koukouli, M. E., Meleti, C., Bais, A., and Zerefos, C.: A study of the total atmospheric sulfur dioxide load using ground-based measurements and the satellite derived Sulfur Dioxide Index, Atmos. Environ., 43, 1693–1701, doi:10.1016/j.atmosenv.2008.12.012, 2009.

Georgoulias, A. K., Kourtidis, K. A., Kosmidis, E., Despotakis, T., and Symeonidis, P.: AMFIC-WSDB: a web data base for hosting and easy retrieval of atmospheric data from satellites, Comput. Geosci., 48, 57–66, doi:10.1016/j.cageo.2012.05.001, 2012.

Georgoulias, A. K., Kourtidis, K. A., Alexandri, G., Rapsomanikis, S., and Sanchez-Lorenzo, A.: Common summertime total cloud cover and aerosol optical depth weekly variabilities over Europe: sign of the aerosol indirect effects?, Atmos. Res., 153, 59–73, doi:10.1016/j.atmosres.2014.07.031, 2015.

Georgoulias, A. K., Alexandri, G., Kourtidis, K. A., Lelieveld, J., Zanis, P., and Amiridis, V.: Differences between the MODIS Collection 6 and 5.1 aerosol datasets over the greater Mediterranean region, Atmos. Environ., 147, 310–319, doi:10.1016/j.atmosenv.2016.10.014, 2016.

Gerasopoulos, E., Kokkalis, P., Amiridis, V., Liakakou, E., Perez, C., Haustein, K., Eleftheratos, K., Andreae, M. O., Andreae, T. W., and Zerefos, C. S.: Dust specific extinction cross-sections over the Eastern Mediterranean using the BSC-DREAM model and sun photometer data: the case of urban environments, Ann. Geophys., 27, 2903–2912, doi:10.5194/angeo-27-2903-2009, 2009.

Gerasopoulos, E., Amiridis, V., Kazadzis, S., Kokkalis, P., Eleftheratos, K., Andreae, M. O., Andreae, T. W., El-Askary, H., and Zerefos, C. S.: Three-year ground based measurements of aerosol optical depth over the Eastern Mediterranean: the urban environment of Athens, Atmos. Chem. Phys., 11, 2145–2159, doi:10.5194/acp-11-2145-2011, 2011.

Ginoux, P., Chin, M., Tegen, I., Prospero, J. M., Holben, B., Dubovik, O., and Lin, S.-J.: Sources and distributions of dust aerosols simulated with the GOCART model, J. Geophys. Res., 106, 20255, doi:10.1029/2000JD000053, 2001.

Ginoux, P., Prospero, J., Torres, O., and Chin, M.: Long-term simulation of global dust distribution with the GOCART model: correlation with North Atlantic Oscillation, Environ. Modell. Softw., 19, 113–128, doi:10.1029/2006GL025734, 2004.

Ginoux, P., Clarisse, L., Clerbaux, C., Coheur, P.-F., Dubovik, O., Hsu, N. C., and Van Damme, M.: Mixing of dust and $NH_3$ observed globally over anthropogenic dust sources, Atmos. Chem. Phys., 12, 7351–7363, doi:10.5194/acp-12-7351-2012, 2012.

Giorgi, F.: Climate change hot-spots, Geophys. Res. Lett., 33, L08707, doi:10.1029/2006GL025734, 2006.

Gkikas, A., Hatzianastassiou, N., and Mihalopoulos, N.: Aerosol events in the broader Mediterranean basin based on 7-year (2000–2007) MODIS C005 data, Ann. Geophys., 27, 3509–3522, doi:10.5194/angeo-27-3509-2009, 2009.

Gkikas, A., Hatzianastassiou, N., Mihalopoulos, N., Katsoulis, V., Kazadzis, S., Pey, J., Querol, X., and Torres, O.: The regime of intense desert dust episodes in the Mediterranean based on contemporary satellite observations and ground measurements, Atmos. Chem. Phys., 13, 12135–12154, doi:10.5194/acp-13-12135-2013, 2013.

Gkikas, A., Houssos, E. E., Lolis, C. J., Bartzokas, A., Mihalopoulos, N., and Hatzianastassiou, N.: Atmospheric circulation evolution related to desert-dust episodes over the Mediterranean, Q. J. Roy. Meteor. Soc., 690, 1634–1645, 2014.

Hatzianastassiou, N., Gkikas, A., Mihalopoulos, N., Torres, O., and Katsoulis, B. D.: Natural versus anthropogenic aerosols in the eastern Mediterranean basin derived from multiyear TOMS and MODIS satellite data, J. Geophys. Res. Atmos., 114, D24202, doi:10.1029/2009JD011982, 2009.

Herman, J. R., Bhartia, P. K., Torres, O., Hsu, C., Seftor, C., and Celarier, E.: Global distribution of UV-absorbing aerosols from Nimbus 7/TOMS data, J. Geophys. Res.-Atmos., 102, 16911–16922, doi:10.1029/96JD03680, 1997.

Herrmann, M., Somot, S., Calmanti, S., Dubois, C., and Sevault, F.: Representation of spatial and temporal variability of daily wind speed and of intense wind events over the Mediterranean Sea using dynamical downscaling: impact of the regional climate model configuration, Nat. Hazards Earth Syst. Sci., 11, 1983–2001, doi:10.5194/nhess-11-1983-2011, 2011.

Holben, B. N., Eck, T. F., Slutsker, I., Tanré, D., Buis, J. P., Setzer, A., Vermote, E., Reagan, J. A., Kaufman, Y. J., Nakajima, T., Lavenu, F., Jankowiak, I., and Smirnov, A.: AERONET – A Federated Instrument Network and Data Archive for

Aerosol Characterization, Remote Sens. Environ., 66, 1–16, doi:10.1016/S0034-4257(98)00031-5, 1998.

Holben, B. N., Tanré, D., Smirnov, A., Eck, T. F., Slutsker, I., Abuhassan, N., Newcomb, W. W., Schafer, J. S., Chatenet, B., Lavenu, F., Kaufman, Y. J., Castle, J. Vande, Setzer, A., Markham, B., Clark, D., Frouin, R., Halthore, R., Karneli, A., O'Neill, N. T., Pietras, C., Pinker, R. T., Voss, K., and Zibordi, G.: An emerging ground-based aerosol climatology: Aerosol optical depth from AERONET, J. Geophys. Res.-Atmos., 106, 12067–12097, doi:10.1029/2001JD900014, 2001.

Hsu, N. C., Tsay, S. C., King, M. D., and Herman, J. R.: Aerosol properties over bright-reflecting source regions, IEEE T. Geosci. Remote, 42, 557–569, doi:10.1109/TGRS.2004.824067, 2004.

Hsu, N. C., Tsay, S. C., King, M. D., and Herman, J. R.: Deep Blue retrievals of Asian aerosol properties during ACE-Asia, IEEE T. Geosci. Remote, 44, 3180–3195, doi:10.1109/TGRS.2006.879540, 2006.

Hsu, N. C., Jeong, M.-J., Bettenhausen, C., Sayer, A. M., Hansell, R., Seftor, C. S., Huang, J., and Tsay, S.-C.: Enhanced Deep Blue aerosol retrieval algorithm: The second generation, J. Geophys. Res.-Atmos., 118, 9296–9315, doi:10.1002/jgrd.50712, 2013.

Huffman, G. J., Bolvin, D. T., Nelkin, E. J., Wolff, D. B., Adler, R. F., Gu, G., Hong, Y., Bowman, K. P., and Stocker, E. F.: The TRMM Multisatellite Precipitation Analysis (TMPA): quasiglobal, multiyear, combined-sensor precipitation estimates at fine scales, J. Hydrometeorol., 8, 38–55, doi:10.1175/JHM560.1, 2007.

Husar, R. B., Prospero, J. M., and Stowe, L. L.: Characterization of tropospheric aerosols over the oceans with the NOAA advanced very high resolution radiometer optical thickness operational product, J. Geophys. Res., 102, 16889–16909, 1997.

Ichoku, C.: A spatio-temporal approach for global validation and analysis of MODIS aerosol products, Geophys. Res. Lett., 29, 8006, doi:10.1029/2001GL013206, 2002.

Ichoku, C., Remer, L. A., and Eck, T. F.: Quantitative evaluation and intercomparison of morning and afternoon Moderate Resolution Imaging Spectroradiometer (MODIS) aerosol measurements from Terra and Aqua, J. Geophys. Res.-Atmos., 110, D10S03, doi:10.1029/2004JD004987, 2005.

Im, U., Markakis, K., Koçak, M., Gerasopoulos, E., Daskalakis, N., Mihalopoulos, N., Poupkou, A., Kındap, T., Unal, A., and Kanakidou, M.: Summertime aerosol chemical composition in the Eastern Mediterranean and its sensitivity to temperature, Atmos. Environ., 50, 164–173, doi:10.1016/j.atmosenv.2011.12.044, 2012.

Inness, A., Baier, F., Benedetti, A., Bouarar, I., Chabrillat, S., Clark, H., Clerbaux, C., Coheur, P., Engelen, R. J., Errera, Q., Flemming, J., George, M., Granier, C., Hadji-Lazaro, J., Huijnen, V., Hurtmans, D., Jones, L., Kaiser, J. W., Kapsomenakis, J., Lefever, K., Leitão, J., Razinger, M., Richter, A., Schultz, M. G., Simmons, A. J., Suttie, M., Stein, O., Thépaut, J.-N., Thouret, V., Vrekoussis, M., Zerefos, C., and the MACC team: The MACC reanalysis: an 8 yr data set of atmospheric composition, Atmos. Chem. Phys., 13, 4073–4109, doi:10.5194/acp-13-4073-2013, 2013.

Israelevich, P., Ganor, E., Alpert, P., Kishcha, P., and Stupp, A.: Predominant transport paths of Saharan dust over the Mediterranean Sea to Europe, J. Geophys. Res., 117, D02205, doi:10.1029/2011JD016482, 2012.

Israelevich, P. L., Levin, Z., Joseph, J. H., and Ganor, E.: Desert aerosol transport in the Mediterranean region as inferred from the TOMS aerosol index, J. Geophys. Res., 107, 4572, doi:10.1029/2001JD002011, 2002.

Israelevich, P. L., Ganor, E., Levin, Z., and Joseph, J. H.: Annual variations of physical properties of desert dust over Israel, J. Geophys. Res., 108, 4381, doi:10.1029/2002JD003163, 2003.

Jones, T. A. and Christopher, S. A.: A reanalysis of MODIS fine mode fraction over ocean using OMI and daily GOCART simulations, Atmos. Chem. Phys., 11, 5805–5817, doi:10.5194/acp-11-5805-2011, 2011.

Kabatas, B., Unal, A., Pierce, R. B., Kindap, T., and Pozzoli, L.: The contribution of Saharan dust in $PM_{10}$ concentration levels in Anatolian Peninsula of Turkey, Sci. Total Environ., 488–489, 413–421, doi:10.1016/j.scitotenv.2013.12.045, 2014.

Kalivitis, N., Gerasopoulos, E., Vrekoussis, M., Kouvarakis, G., Kubilay, N., Hatzianastassiou, N., Vardavas, I., and Mihalopoulos, N.: Dust transport over the eastern Mediterranean derived from Total Ozone Mapping Spectrometer, Aerosol Robotic Network, and surface measurements, J. Geophys. Res., 112, D03202, doi:10.1029/2006JD007510, 2007.

Kanakidou, M., Mihalopoulos, N., Kindap, T., Im, U., Vrekoussis, M., Gerasopoulos, E., Dermitzaki, E., Unal, A., Koçak, M., Markakis, K., Melas, D., Kouvarakis, G., Youssef, A. F., Richter, A., Hatzianastassiou, N., Hilboll, A., Ebojie, F., Wittrock, F., von Savigny, C., Burrows, J. P., Ladstaetter-Weissenmayer, A., and Moubasher, H.: Megacities as hot spots of air pollution in the East Mediterranean, Atmos. Environ., 45, 1223–1235, doi:10.1016/j.atmosenv.2010.11.048, 2011.

Karnieli, A., Derimian, Y., Indoitu, R., Panov, N., Levy, R. C., Remer, L. A., Maenhaut, W., and Holben, B. N.: Temporal trend in anthropogenic sulfur aerosol transport from central and eastern Europe to Israel, J. Geophys. Res., 114, D00D19, doi:10.1029/2009JD011870, 2009.

Kaskaoutis, D. G., Kosmopoulos, P., Kambezidis, H. D., and Nastos, P. T.: Aerosol climatology and discrimination of different types over Athens, Greece, based on MODIS data, Atmos. Environ., 41, 7315–7329, doi:10.1016/j.atmosenv.2007.05.017, 2007.

Kaskaoutis, D. G., Kambezidis, H. D., Nastos, P. T., and Kosmopoulos, P. G.: Study on an intense dust storm over Greece, Atmos. Environ., 42, 6884–6896, doi:10.1016/j.atmosenv.2008.05.017, 2008.

Kaskaoutis, D. G., Nastos, P. T., Kosmopoulos, P. G., and Kambezidis, H. D.: The combined use of satellite data, air-mass trajectories and model applications for monitoring dust transport over Athens, Greece, Int. J. Remote Sens., 31, 5089–5109, doi:10.1080/01431160903283868, 2010.

Kaskaoutis, D. G., Kharol, S. K., Sifakis, N., Nastos, P. T., Sharma, A. R., Badarinath, K. V. S., and Kambezidis, H. D.: Satellite monitoring of the biomass-burning aerosols during the wildfires of August 2007 in Greece: Climate implications, Atmos. Environ., 45, 716–726, doi:10.1016/j.atmosenv.2010.09.043, 2011.

Kaskaoutis, D. G., Kosmopoulos, P. G., Nastos, P. T., Kambezidis, H. D., Sharma, M., and Mehdi, W.: Transport pathways of Sahara dust over Athens, Greece as detected by MODIS and TOMS, Geomatics, Nat. Hazards Risk, 3, 35–54, doi:10.1080/19475705.2011.574296, 2012a.

Kaskaoutis, D. G., Prasad, A. K., Kosmopoulos, P. G., Sinha, P. R., Kharol, S. K., Gupta, P., El-Askary, H. M., and Kafatos,

M.: Synergistic use of remote sensing and modeling for tracing dust storms in the mediterranean, Adv. Meteorol., 2012, 1–14, doi:10.1155/2012/861026, 2012b.

Kaskaoutis, D. G., Nastos, P. T., Kosmopoulos, P. G., and Kambezidis, H. D.: Characterising the long-range transport mechanisms of different aerosol types over Athens, Greece during 2000–2005, Int. J. Climatol., 32, 1249–1270, doi:10.1002/joc.2357, 2012c.

Kaskaoutis, D. G., Kahn, R. A., Pawan Gupta, P., Jayaraman, A., and Bartzokas, A.: Desert Dust Properties, Modelling, and Monitoring, Adv. Meteorol., 2012, 483632, doi:10.1155/2012/483632, 2012d.

Kaufman, Y. J., Tanré, D., Remer, L. A., Vermote, E. F., Chu, A., and Holben, B. N.: Operational remote sensing of tropospheric aerosol over land from EOS moderate resolution imaging spectroradiometer, J. Geophys. Res., 102, 17051, doi:10.1029/96JD03988, 1997.

Kaufman, Y. J., Koren, I., Remer, L. A., Tanré, D., Ginoux, P., and Fan, S.: Dust transport and deposition observed from the Terra-Moderate Resolution Imaging Spectroradiometer (MODIS) spacecraft over the Atlantic Ocean, J. Geophys. Res.-Atmos., 110, D10S12, doi:10.1029/2003JD004436, 2005.

Kazadzis, S., Bais, A., Amiridis, V., Balis, D., Meleti, C., Kouremeti, N., Zerefos, C. S., Rapsomanikis, S., Petrakakis, M., Kelesis, A., Tzoumaka, P., and Kelektsoglou, K.: Nine years of UV aerosol optical depth measurements at Thessaloniki, Greece, Atmos. Chem. Phys., 7, 2091–2101, doi:10.5194/acp-7-2091-2007, 2007.

Kazadzis, S., Veselovskii, I., Amiridis, V., Gröbner, J., Suvorina, A., Nyeki, S., Gerasopoulos, E., Kouremeti, N., Taylor, M., Tsekeri, A., and Wehrli, C.: Aerosol microphysical retrievals from precision filter radiometer direct solar radiation measurements and comparison with AERONET, Atmos. Meas. Tech., 7, 2013–2025, doi:10.5194/amt-7-2013-2014, 2014.

Kelektsoglou, K. and Rapsomanikis, S.: AERONET observations of direct and indirect aerosol effects over a South European conurbation, Int. J. Remote Sens., 32, 2779–2798, 2011.

Khaliq, M. N. and Ouarda, T. B. M. J.: On the critical values of the standard normal homogeneity test (SNHT), Int. J. Climatol., 27, 681–687, doi:10.1002/joc.1438, 2007.

Kloog, I., Sorek-Hamer, M., Lyapustin, A., Coull, B., Wang, Y., Just, A. C., Schwartz, J., and Broday, D. M.: Estimating daily $PM_{2.5}$ and $PM_{10}$ across the complex geo-climate region of Israel using MAIAC satellite-based AOD data, Atmos. Environ., 122, 409–416, doi:10.1016/j.atmosenv.2015.10.004, 2015.

Kokkalis, P., Papayannis, A., Amiridis, V., Mamouri, R. E., Veselovskii, I., Kolgotin, A., Tsaknakis, G., Kristiansen, N. I., Stohl, A., and Mona, L.: Optical, microphysical, mass and geometrical properties of aged volcanic particles observed over Athens, Greece, during the Eyjafjallajökull eruption in April 2010 through synergy of Raman lidar and sunphotometer measurements, Atmos. Chem. Phys., 13, 9303–9320, doi:10.5194/acp-13-9303-2013, 2013.

Koren, I., Joseph, J. H., and Israelevich P.: Detection of dust plumes and their sources in northeastern Libya, Can. J. Remote Sens., 29, 792–796, 2003.

Kosmopoulos, P. G., Kaskaoutis, D. G., Nastos, P. T., and Kambezidis, H. D.: Seasonal variation of columnar aerosol optical properties over Athens, Greece, based on MODIS data, Remote Sens. Environ., 112, 2354–2366, doi:10.1016/j.rse.2007.11.006, 2008.

Koukouli, M., Balis, D., Amiridis, V., Kazadzis, S., Bais, A., Nickovic, S., and Torres, O.: Aerosol variability over Thessaloniki using ground based remote sensing observations and the TOMS aerosol index, Atmos. Environ., 40, 5367–5378, doi:10.1016/j.atmosenv.2006.04.046, 2006.

Koukouli, M. E., Kazadzis, S., Amiridis, V., Ichoku, C., and Balis, D. S.: Comparisons of satellite derived aerosol optical depth over a variety of sites in the southern Balkan region as an indicator of local air quality, Remote sensing of clouds and the atmosphere XII, edited by: Comerón, A., Picard, R. H., Schäfer, K., Slusser, J. R., and Amodeo, A., Proceedings of SPIE, Vol. 67451V, doi:10.1117/12.737681, 2007.

Koukouli, M. E., Kazadzis, S., Amiridis, V., Ichoku, C., Balis, D. S., and Bais, A. F.: Signs of a negative trend in the MODIS aerosol optical depth over the Southern Balkans, Atmos. Environ., 44, 1219–1228, doi:10.1016/j.atmosenv.2009.11.024, 2010.

Kourtidis, K., Rapsomanikis, S., Zerefos, C., Georgoulias, A. K., and Pavlidou E.: Severe particulate pollution from the deposition practices of the primary materials of a cement plant, Environ. Sci. Pollut. R., 21, 9796–9808, doi:10.1007/s11356-014-2969-6, 2014.

Kourtidis, K., Stathopoulos, S., Georgoulias, A. K., Alexandri, G., and Rapsomanikis, S.: A study of the impact of synoptic weather conditions and water vapor on aerosol-cloud relationships over major urban clusters of China, Atmos. Chem. Phys., 15, 10955–10964, doi:10.5194/acp-15-10955-2015, 2015.

Kubilay, N.: Optical properties of mineral dust outbreaks over the northeastern Mediterranean, J. Geophys. Res., 108, 4666, doi:10.1029/2003JD003798, 2003.

Lehahn, Y., Koren, I., Boss, E., Ben-Ami, Y., and Altaratz, O.: Estimating the maritime component of aerosol optical depth and its dependency on surface wind speed using satellite data, Atmos. Chem. Phys., 10, 6711–6720, doi:10.5194/acp-10-6711-2010, 2010.

Lelieveld, J., Berresheim, H., Borrmann, S., Crutzen, P. J., Dentener, F. J., Fischer, H., Feichter, J., Flatau, P. J., Heland, J., Holzinger, R., Korrmann, R., Lawrence, M. G., Levin, Z., Markowicz, K. M., Mihalopoulos, N., Minikin, A., Ramanathan, V., De Reus, M., Roelofs, G. J., Scheeren, H. A., Sciare, J., Schlager, H., Schultz, M., Siegmund, P., Steil, B., Stephanou, E. G., Stier, P., Traub, M., Warneke, C., Williams, J., and Ziereis, H.: Global air pollution crossroads over the Mediterranean, Science, 298, 794–799, doi:10.1126/science.1075457, 2002.

Levelt, P. F., Van den Oord, G. H. J., Dobber, M. R., Malkki, A., Visser, H., de Vries, J., Stammes, P., Lundell, J. O. V., and Saari, H.: The Ozone Monitoring Instrument, IEEE T. Geosci. Remote, 44, 1093–1101, 2006.

Levy, R. C., Remer, L. A., Tanré, D., Kaufman, Y. J., Ichoku, C., Holben, B. N., Livingston, J. M., Russell, P. B., and Maring, H.: Evaluation of the Moderate-Resolution Imaging Spectroradiameter (MODIS) retrievals of dust aerosol over the ocean during PRIDE, J. Geophys. Res., 108, 8594, doi:10.1029/2002JD002460, 2003.

Levy, R. C., Remer, L. A., and Dubovik, O.: Global aerosol optical properties and application to Moderate Resolution Imaging Spectroradiometer aerosol retrieval over land, J. Geophys. Res.-Atmos., 112, D13210, doi:10.1029/2006JD007815, 2007a.

Levy, R. C., Remer, L. A., Mattoo, S., Vermote, E. F., and Kaufman, Y. J.: Second-generation operational algorithm: Retrieval of aerosol properties over land from inversion of Moderate Resolution Imaging Spectroradiometer spectral reflectance, J. Geophys. Res.-Atmos., 112, D13211, doi:10.1029/2006JD007811, 2007b.

Levy, R., Remer, L., Tanré, D., Mattoo, S., and Kaufman, Y.: Algorithm for remote sensing of tropospheric aerosol over dark targets from MODIS: Collections 005 and 051: Revision 2, February 2009, MODIS Algorithm Theoretical Basis Document, 2009.

Levy, R. C., Remer, L. A., Kleidman, R. G., Mattoo, S., Ichoku, C., Kahn, R., and Eck, T. F.: Global evaluation of the Collection 5 MODIS dark-target aerosol products over land, Atmos. Chem. Phys., 10, 10399–10420, doi:10.5194/acp-10-10399-2010, 2010.

Levy, R. C., Mattoo, S., Munchak, L. A., Remer, L. A., Sayer, A. M., Patadia, F., and Hsu, N. C.: The Collection 6 MODIS aerosol products over land and ocean, Atmos. Meas. Tech., 6, 2989–3034, doi:10.5194/amt-6-2989-2013, 2013.

Li, C., Joiner, J., Krotkov, N. A., and Bhartia, P. K.: A fast and sensitive new satellite $SO_2$ retrieval algorithm based on principal component analysis: Application to the ozone monitoring instrument, Geophys. Res. Lett., 40, 6314–6318, doi:10.1002/2013GL058134, 2013.

Li, J., Carlson, B. E., and Lacis, A. A.: A study on the temporal and spatial variability of absorbing aerosols using Total Ozone Mapping Spectrometer and Ozone Monitoring Instrument Aerosol Index data, J. Geophys. Res., 114, D09213, doi:10.1029/2008JD011278, 2009.

Li, J., Carlson, B. E., Dubovik, O., and Lacis, A. A.: Recent trends in aerosol optical properties derived from AERONET measurements, Atmos. Chem. Phys., 14, 12271–12289, doi:10.5194/acp-14-12271-2014, 2014.

Liora, N., Markakis, K., Poupkou, A., Giannaros, T. M., and Melas, D.: The natural emissions model (NEMO): Description, application and model evaluation, Atmos. Environ., 122, 493–504, doi:10.1016/j.atmosenv.2015.10.014, 2015.

Lyapustin, A., Wang, Y., Xiong, X., Meister, G., Platnick, S., Levy, R., Franz, B., Korkin, S., Hilker, T., Tucker, J., Hall, F., Sellers, P., Wu, A., and Angal, A.: Scientific impact of MODIS C5 calibration degradation and C6+ improvements, Atmos. Meas. Tech., 7, 4353–4365, doi:10.5194/amt-7-4353-2014, 2014.

Mamouri, R. E., Amiridis, V., Papayannis, A., Giannakaki, E., Tsaknakis, G., and Balis, D. S.: Validation of CALIPSO space-borne-derived attenuated backscatter coefficient profiles using a ground-based lidar in Athens, Greece, Atmos. Meas. Tech., 2, 513–522, doi:10.5194/amt-2-513-2009, 2009.

Mamouri, R. E., Ansmann, A., Nisantzi, A., Kokkalis, P., Schwarz, A., and Hadjimitsis, D.: Low Arabian extinctionto-backscatter ratio, Geophys. Res. Lett., 40, 4762–4766, doi:10.1002/grl.50898, 2013.

Mamouri, R. E. and Ansmann, A.: Estimated desert-dust ice nuclei profiles from polarization lidar: methodology and case studies, Atmos. Chem. Phys., 15, 3463–3477, doi:10.5194/acp-15-3463-2015, 2015.

Mangold, A., De Backer, H., De Paepe, B., Dewitte, S., Chiapello, I., Derimian, Y., Kacenelenbogen, M., Léon, J.-F., Huneeus, N., Schulz, M., Ceburnis, D., O'Dowd, C., Flentje, H., Kinne, S., Benedetti, A., Morcrette, J.-J., and Boucher, O.: Aerosol analysis and forecast in the European Centre for Medium-Range Weather Forecasts Integrated Forecast System: 3. Evaluation by means of case studies, J. Geophys. Res., 116, D03302, doi:10.1029/2010JD014864, 2011.

Marey, H. S., Gille, J. C., El-Askary, H. M., Shalaby, E. A., and El-Raey, M. E.: Aerosol climatology over Nile Delta based on MODIS, MISR and OMI satellite data, Atmos. Chem. Phys., 11, 10637–10648, doi:10.5194/acp-11-10637-2011, 2011.

Mateos, D., Antón, M., Toledano, C., Cachorro, V. E., Alados-Arboledas, L., Sorribas, M., Costa, M. J., and Baldasano, J. M.: Aerosol radiative effects in the ultraviolet, visible, and near-infrared spectral ranges using long-term aerosol data series over the Iberian Peninsula, Atmos. Chem. Phys., 14, 13497–13514, doi:10.5194/acp-14-13497-2014, 2014.

Mélin, F., Zibordi, G. and Djavidnia, S.: Development and validation of a technique for merging satellite derived aerosol optical depth from SeaWiFS and MODIS, Remote Sens. Environ., 108, 436–450, doi:10.1016/j.rse.2006.11.026, 2007.

Mishra, A. K., Klingmueller, K., Fredj, E., Lelieveld, J., Rudich, Y., and Koren, I.: Radiative signature of absorbing aerosol over the eastern Mediterranean basin, Atmos. Chem. Phys., 14, 7213–7231, doi:10.5194/acp-14-7213-2014, 2014.

Morcrette, J.-J., Boucher, O., Jones, L., Salmond, D., Bechtold, P., Beljaars, A., Benedetti, A., Bonet, A., Kaiser, J. W., Razinger, M., Schulz, M., Serrar, S., Simmons, A. J., Sofiev, M., Suttie, M., Tompkins, A. M., and Untch, A.: Aerosol analysis and forecast in the European Centre for Medium-Range Weather Forecasts Integrated Forecast System: Forward modeling, J. Geophys. Res., 114, D06206, doi:10.1029/2008JD011235, 2009.

Moulin, C., Lambert, C. E., Dayan, U., Masson, V., Ramonet, M., Bousquet, P., Legrand, M., Balkanski, Y. J., Guelle, W., Marticorena, B., Bergametti, G., and Dulac, F.: Satellite climatology of African dust transport in the Mediterranean atmosphere, J. Geophys. Res.-Atmos., 103, 13137–13144, doi:10.1029/98JD00171, 1998.

Nabat, P., Solmon, F., Mallet, M., Kok, J. F., and Somot, S.: Dust emission size distribution impact on aerosol budget and radiative forcing over the Mediterranean region: a regional climate model approach, Atmos. Chem. Phys., 12, 10545–10567, doi:10.5194/acp-12-10545-2012, 2012.

Nabat, P., Somot, S., Mallet, M., Chiapello, I., Morcrette, J. J., Solmon, F., Szopa, S., Dulac, F., Collins, W., Ghan, S., Horowitz, L. W., Lamarque, J. F., Lee, Y. H., Naik, V., Nagashima, T., Shindell, D., and Skeie, R.: A 4-D climatology (1979–2009) of the monthly tropospheric aerosol optical depth distribution over the Mediterranean region from a comparative evaluation and blending of remote sensing and model products, Atmos. Meas. Tech., 6, 1287–1314, doi:10.5194/amt-6-1287-2013, 2013.

Nikitidou, E. and Kazantzidis, A.: On the differences of ultraviolet and visible irradiance calculations in the Mediterranean basin due to model- and satellite-derived climatologies of aerosol optical properties, Int. J. Climatol., 33, 2877–2888, doi:10.1002/joc.3638, 2013.

Nisantzi, A., Mamouri, R. E., Ansmann, A., Schuster, G. L., and Hadjimitsis, D. G.: Middle East versus Saharan dust extinction-to-backscatter ratios, Atmos. Chem. Phys., 15, 7071–7084, doi:10.5194/acp-15-7071-2015, 2015.

Papadimas, C. D., Hatzianastassiou, N., Mihalopoulos, N., Querol, X., and Vardavas, I.: Spatial and temporal variability in aerosol properties over the Mediterranean basin based on 6-

year (2000–2006) MODIS data, J. Geophys. Res., 113, D11205, doi:10.1029/2007JD009189, 2008.

Papadimas, C. D., Hatzianastassiou, N., Mihalopoulos, N., Kanakidou, M., Katsoulis, B. D., and Vardavas, I.: Assessment of the MODIS Collections C005 and C004 aerosol optical depth products over the Mediterranean basin, Atmos. Chem. Phys., 9, 2987–2999, doi:10.5194/acp-9-2987-2009, 2009.

Papadimas, C. D., Hatzianastassiou, N., Matsoukas, C., Kanakidou, M., Mihalopoulos, N., and Vardavas, I.: The direct effect of aerosols on solar radiation over the broader Mediterranean basin, Atmos. Chem. Phys., 12, 7165–7185, doi:10.5194/acp-12-7165-2012, 2012.

Papayannis, A. and Balis, D.: Study of the structure of the lower troposphere over Athens using a backscattering Lidar during the MEDCAPHOT-TRACE experiment: Measurements over a suburban area, Atmos. Environ., 32, 2161–2172, 1998.

Papayannis, A., Balis, D., Amiridis, V., Chourdakis, G., Tsaknakis, G., Zerefos, C., Castanho, A. D. A., Nickovic, S., Kazadzis, S., and Grabowski, J.: Measurements of Saharan dust aerosols over the Eastern Mediterranean using elastic backscatter-Raman lidar, spectrophotometric and satellite observations in the frame of the EARLINET project, Atmos. Chem. Phys., 5, 2065–2079, doi:10.5194/acp-5-2065-2005, 2005.

Papayannis, A., Mamouri, R. E., Amiridis, V., Kazadzis, S., Pérez, C., Tsaknakis, G., Kokkalis, P., and Baldasano, J. M.: Systematic lidar observations of Saharan dust layers over Athens, Greece in the frame of EARLINET project (2004–2006), Ann. Geophys., 27, 3611–3620, doi:10.5194/angeo-27-3611-2009, 2009.

Pey, J., Querol, X., Alastuey, A., Forastiere, F., and Stafoggia, M.: African dust outbreaks over the Mediterranean Basin during 2001–2011: $PM_{10}$ concentrations, phenomenology and trends, and its relation with synoptic and mesoscale meteorology, Atmos. Chem. Phys., 13, 1395–1410, doi:10.5194/acp-13-1395-2013, 2013.

Pozzer, A., de Meij, A., Yoon, J., Tost, H., Georgoulias, A. K., and Astitha, M.: AOD trends during 2001–2010 from observations and model simulations, Atmos. Chem. Phys., 15, 5521–5535, doi:10.5194/acp-15-5521-2015, 2015.

Rea, G., Turquety, S., Menut, L., Briant, R., Mailler, S., and Siour, G.: Source contributions to 2012 summertime aerosols in the Euro-Mediterranean region, Atmos. Chem. Phys., 15, 8013–8036, doi:10.5194/acp-15-8013-2015, 2015.

Remer, L. A., Tanre, D., Kaufman, Y. J., Ichoku, C., Mattoo, S., Levy, R., Chu, D. A., Holben, B., Dubovik, O., Smirnov, A., Martins, J. V., Li, R. R., and Ahmad, Z.: Validation of MODIS aerosol retrieval over ocean, Geophys. Res. Lett., 29, 2–5, doi:10.1029/2001GL013204, 2002.

Remer, L. A., Kaufman, Y. J., Tanré, D., Mattoo, S., Chu, D. A., Martins, J. V., Li, R.-R., Ichoku, C., Levy, R. C., Kleidman, R. G., Eck, T. F., Vermote, E., and Holben, B. N.: The MODIS Aerosol Algorithm, Products, and Validation, J. Atmos. Sci., 62, 947–973, doi:10.1175/JAS3385.1, 2005.

Remer, L., Kaufman, Y., and Kleidman, R.: Comparison of three years of terra and aqua MODIS aerosol optical thickness over the global oceans, IEEE Geosci. Remote S., 3, 537–540, doi:10.1109/LGRS.2006.879562, 2006.

Remer, L. A., Kleidman, R. G., Levy, R. C., Kaufman, Y. J., Tanré, D., Mattoo, S., Martins, J. V., Ichoku, C., Koren, I., Yu, H., and Holben, B. N.: Global aerosol climatology from the MODIS satellite sensors, J. Geophys. Res., 113, D14S07, doi:10.1029/2007JD009661, 2008.

Retalis, A. and Sifakis, N.: Urban aerosol mapping over Athens using the differential textural analysis (DTA) algorithm on MERIS-ENVISAT data, ISPRS J. Photogramm. Remote Sens., 65, 17–25, doi:10.1016/j.isprsjprs.2009.08.001, 2010.

Rudich, Y., Kaufman, Y. J., Dayan, U., Yu, H., and Kleidman, R. G.: Estimation of transboundary transport of pollution aerosols by remote sensing in the eastern Mediterranean, J. Geophys. Res., 113, D14S14, doi:10.1029/2007JD009601, 2008.

Sayer, A. M., Hsu, N. C., Bettenhausen, C., and Jeong, M. J.: Validation and uncertainty estimates for MODIS Collection 6 "deep Blue" aerosol data, J. Geophys. Res.-Atmos., 118, 7864–7872, doi:10.1002/jgrd.50600, 2013.

Sayer, A. M., Munchak, L. A., Hsu, N. C., Levy, R. C., Bettenhausen, C., and Jeong, M.-J.: MODIS Collection 6 aerosol products: Comparison between Aqua's e-Deep Blue, Dark Target, and "merged" data sets, and usage recommendations, J. Geophys. Res.-Atmos., 119, 13965–13989, doi:10.1002/2014JD022453, 2014.

Sciare, J., Oikonomou, K., Favez, O., Liakakou, E., Markaki, Z., Cachier, H., and Mihalopoulos, N.: Long-term measurements of carbonaceous aerosols in the Eastern Mediterranean: evidence of long-range transport of biomass burning, Atmos. Chem. Phys., 8, 5551–5563, doi:10.5194/acp-8-5551-2008, 2008.

Shi, Y., Zhang, J., Reid, J. S., Holben, B., Hyer, E. J., and Curtis, C.: An analysis of the collection 5 MODIS over-ocean aerosol optical depth product for its implication in aerosol assimilation, Atmos. Chem. Phys., 11, 557–565, doi:10.5194/acp-11-557-2011, 2011.

Shi, Y., Zhang, J., Reid, J. S., Hyer, E. J., and Hsu, N. C.: Critical evaluation of the MODIS Deep Blue aerosol optical depth product for data assimilation over North Africa, Atmos. Meas. Tech., 6, 949–969, doi:10.5194/amt-6-949-2013, 2013.

Sifakis, N. I., Iossifidis, C., and Kontoes, C.: CHRISTINE Code for High ResolutIon Satellite mapping of optical ThIckness and ÅNgstrom Exponent. Part II: First application to the urban area of Athens, Greece and comparison to results from previous contrast-reduction codes, Comput. Geosci., 62, 142–149, doi:10.1016/j.cageo.2013.05.011, 2014.

Smirnov, A.: Maritime component in aerosol optical models derived from Aerosol Robotic Network data, J. Geophys. Res., 108, 4033, doi:10.1029/2002JD002701, 2003.

Sorek-Hamer, M., Cohen, A., Levy, R. C., Ziv, B., and Broday, D. M.: Classification of dust days by satellite remotely sensed aerosol products, Int. J. Remote Sens., 34, 2672–2688, doi:10.1080/01431161.2012.748991, 2013.

Tanré, D., Kaufman, Y. J., Herman, M., and Mattoo, S.: Remote sensing of aerosol properties over oceans using the MODIS/EOS spectral radiances, J. Geophys. Res.-Atmos., 102, 16971–16988, doi:10.1029/96JD03437, 1997.

Torres, O., Bhartia, P. K., Herman, J. R., Ahmad, Z., and Gleason, J.: Derivation of aerosol properties from a satellite measurements of backscattered ultraviolet radiation: Theoretical basis, J. Geophys. Res., 103, 17099–17110, 1998.

Torres, O., Tanskanen, A., Veihelman, B., Ahn, C., Braak, R., Bhartia, P. K., Veefkind, P., and Levelt, P.: Aerosols and Surface UV Products from OMI Observations: An Overview, J. Geophys. Res., 112, D24S47, doi:10.1029/2007JD008809, 2007.

Tsaknakis, G., Papayannis, A., Kokkalis, P., Amiridis, V., Kambezidis, H. D., Mamouri, R. E., Georgoussis, G., and Avdikos, G.: Inter-comparison of lidar and ceilometer retrievals for aerosol and Planetary Boundary Layer profiling over Athens, Greece, Atmos. Meas. Tech., 4, 1261–1273, doi:10.5194/amt-4-1261-2011, 2011.

Tyrlis, E. and Lelieveld, J.: Climatology and dynamics of the summer Etesian winds over the Eastern Mediterranean, J. Atmos. Sci., 70, 3374–3396, doi:10.1175/JAS-D-13-035.1, 2013.

Varga, G., Ujvari, G., and Kovacs, J.: Spatiotemporal patterns of Saharan dust outbreaks in the Mediterranean Basin, Aeolian Res., 15, 151–160, doi:10.1016/j.aeolia.2014.06.005, 2014.

Vrekoussis, M., Liakakou, E., Koçak, M., Kubilay, N., Oikonomou, K., Sciare, J., and Mihalopoulos, N.: Seasonal variability of optical properties of aerosols in the Eastern Mediterranean, Atmos. Environ., 39, 7083–7094, doi:10.1016/j.atmosenv.2005.08.011, 2005.

Zyrichidou, I., Koukouli, M. E., Balis, D. S., Katragkou, E., Melas, D., Poupkou, A., Kioutsioukis, I., van der A, R., Boersma, F. K., van Roozendael, M., and Richter, A.: Satellite observations and model simulations of tropospheric $NO_2$ columns over south-eastern Europe, Atmos. Chem. Phys., 9, 6119–6134, doi:10.5194/acp-9-6119-2009, 2009.